AFOSR-TR- 89-0045

SC5444.FR

SC5444.FR

Copy No. 4

TRANSFORMATION TOUGHENING OF CERAMICS

FINAL REPORT FOR THE PERIOD
September 1, 1985 through August 31, 1988

CONTRACT NO. F49620-85-C-0143

Prepared for

Air Force Office of Scientific Research
Directorate of Electronic and Material Sciences
Building 410
Bolling AFB, Washington, DC 20332-6448

D.B. Marshall
Principal Investigator

DECEMBER 1988

Rockwell International
Science Center

UNCLASSIFIED

SECURITY CLASSIFICATION OF THIS PAGE

REPORT DOCUMENTATION PAGE

FORM APPROVED OMB No. 0704-0188

1a. REPORT SECURITY CLASSIFICATION UNCLASSIFIED	1b. RESTRICTIVE MARKINGS
2a. SECURITY CLASSIFICATION AUTHORITY	3. DISTRIBUTION/AVAILABILITY OF REPORT Approved for public release; distribution is unlimited
2b. CLASSIFICATION/DOWNGRADING SCHEDULE	
4. PERFORMING ORGANIZATION REPORT NUMBER(S) SC5444.FR	5. MONITORING ORGANIZATION REPORT NUMBER(S) AFOSR-TR- 89-0045
6a. NAME OF PERFORMING ORGANIZATION ROCKWELL INTERNATIONAL Science Center 6b. OFFICE SYMBOL (If Applicable)	7a. NAME OF MONITORING ORGANIZATION AFOSR
6c. ADDRESS (City, State, and ZIP Code) 1049 Camino Dos Rios Thousand Oaks, CA 91360	7b. ADDRESS (City, State and ZIP Code) BLDG 410 BAFB DC 20332-6448
8a. NAME OF FUNDING/SPONSORING ORGANIZATION Air Force Office of Scientific Research 8b. OFFICE SYMBOL (If Applicable) NE	9. PROCUREMENT INSTRUMENT IDENTIFICATION NUMBER CONTRACT NO. F49620-85-C-0143
8c. ADDRESS (City, State and ZIP Code) Directorate of Electronic & Material Sciences Building 410 Bolling AFB, DC 20332-6448	10. SOURCE OF FUNDING NOS. PROGRAM ELEMENT NO. 61102F PROJECT NO. 2306/A2 TASK NO. A2 WORK UNIT ACCESSION NO.
11. TITLE (Include Security Classification) TRANSFORMATION TOUGHENING OF CERAMICS	
12. PERSONAL AUTHOR(S) Marshall, D.B.	
13a. TYPE OF REPORT Final Report	13b. TIME COVERED FROM 09/01/85 TO 08/31/88 14. DATE OF REPORT (Year, Month, Day) 1988, DECEMBER 15. PAGE COUNT
16. SUPPLEMENTARY NOTATION	

17. COSATI CODES			18. SUBJECT TERMS (Continue on reverse if necessary and identify by block number)
FIELD	GROUP	SUB-GROUP	

19. ABSTRACT (Continue on reverse if necessary and identify by block number)

The results of a three-year study, aimed at understanding factors that dictate microstructural evolution and mechanical properties of transformation toughened ceramics, are summarized. Large crack growth resistance curves (rather than single valued toughness) were discovered in toughened zirconia, and these were shown to be responsible for strength-toughness relations, damage tolerance, and other mechanical properties. New insight was gained into mechanisms of controlling grain growth during processing, and a method for forming high strength, fine grained ZrO_2 fibers was discovered. In the final year's work, which is reported in detail here, a new tetragonal-to-orthorhombic phase transformation at low temperatures was discovered and shown to have a dramatic effect on mechanical properties. New methods were ap-

20. DISTRIBUTION/AVAILABILITY OF ABSTRACT UNCLASSIFIED/UNLIMITED ☐ SAME AS RPT. ☒ DTIC USERS ☐	21. ABSTRACT SECURITY CLASSIFICATION UNCLASSIFIED
22a. NAME OF RESPONSIBLE INDIVIDUAL Dr. L.J. Schioler	22b. TELEPHONE NUMBER (Include Area Code) (202) 767-4933 22c. OFFICE SYMBOL NE

DD FORM 1473, JUN 86 Previous editions are obsolete.

UNCLASSIFIED

SECURITY CLASSIFICATION OF THIS PAGE

plied to measure the amount and location of phase transformation within crack tip zones and to quantify crack tip shielding, evaluate stability and reversibility of the martensitic transformation, and to determine the net transformation strain that gives to toughening. Finally, crack growth under cyclic loading was demonstrated to be important in zirconia materials. (JES) ←

TABLE OF CONTENTS

ABSTRACT

The results of a three-year study, aimed at understanding factors that dictate microstructural evolution and mechanical properties of transformation toughened ceramics, are summarized. Large crack growth resistance curves (rather than single valued toughness) were discovered in toughened zirconia, and these were shown to be responsible for strength-toughness relations, damage tolerance, and other mechanical properties. New insight was gained into mechanisms of controlling grain growth during processing, and a method for forming high strength, fine grained ZrO_2 fibers was discovered. In the final year's work, which is reported in detail here, a new tetragonal-to-orthorhombic phase transformation at low temperatures was discovered and shown to have a dramatic effect on mechanical properties. New methods were applied to measure the amount and location of phase transformation within crack tip zones and to quantify crack tip shielding, evaluate stability and reversibility of the martensitic transformation, and to determine the net transformation strain that gives rise to toughening. Finally, crack growth under cyclic loading was demonstrated to be important in zirconia materials.

1.0 INTRODUCTION

The goal of this research is to develop a basic scientific understanding of the factors that dictate microstructural evolution and mechanical properties of transformation-toughened ceramics, in order to enable development of new transformation-toughened materials with higher temperature capabilities than existing systems. The work has focused on two main topics. One is the understanding of transformation mechanisms and relations between the microstructural characteristics and macroscopic mechanical properties such as strength and toughness. This involves micromechanics modeling based on in situ observations of damage development mechanisms and toughening mechanisms. The other is the control of microstructure during sintering, especially involving the role of second phases and phase partitioning in controlling grain growth. Detailed results of the research done during the past year are contained in four papers that are included as Sections 3 to 6 of this report, and which will be submitted to, or have been published in, the journals or books noted on the title pages. A complete list of publications from the three-year program is included as Section 2. The results are summarized briefly below.

During the first two years we discovered some new concepts that changed our understanding of relations between strength, toughness, and optimum microstructures, as well as giving new insight into routes for controlling microstructure. These include the following:

1. The existence of a crack growth resistance curve (R-curve) rather than a single-valued fracture toughness. This has many important implications because the strength can be dictated by the R-curve rather than by preexisting flaws and a degree of damage tolerance is thus exhibited. In that case, new criteria are needed for prediction of reliability, because existing approaches used for brittle materials design (statistical theories of strength and theories of delayed failure and proof testing) do not apply. The relation beteen R-curves and strength/toughness relations was analyzed; the slope of the R-curve rather than the steady-state fracture toughness was shown to dictate the strength of the material, and the analysis accounted for the general trend, observed in several transformation-toughened material systems, that the peak strength is achieved at intermediate fracture toughness rather than at the peak toughness. This was confirmed experimentally by measuring R-curves and strength-toughness relations (as well as

stress-strain curves and in situ observations of transformation stability) in a series of Mg-PSZ materials in which the amount of transformation toughening could be varied systematically over a wide range by sub eutectoid heat treatment, without substantially changing microstructural properties such as grain size and precipitate size and morphology.

2. The key to obtaining high fracture toughness and extensive R-curve growth was shown to lie in the stabilization of the martensitic tetragonal-monoclinic transformation rather than the conventional idea that it is the initiation of the transformation that is most important. Under increasing applied stress the transformation was found to occur reversibly at low stresses but at higher applied stress the transformation became irreversible. Moreover the stress required for initiation of reversible transformation was independent of the heat treatment, over a range of treatment times that caused toughness variations from ~ 7 MPa $m^{1/2}$ to 15 MPa $m^{1/2}$, whereas the stress required for permanent transformation decreased with increasing toughness. Detailed in situ observations were used to examine the nature of (and correlation between) reversible and irreversible transformations in various stress states. These observations provided a basis for suggesting mechanisms of transformation nucleation and stabilization - the critical factor which determines the fracture toughness and strength properties of transformation toughened ceramics.

3. Mechanisms of controlling microstructure, phase content, and grain growth by processing in multiphase regions have been elucidated. Using the system Y_2O_3-ZrO_2, specimens with extremely uniform initial compositional distributions were fabricated from a metastable organo-metallic precursor, obtained by mixing solutions of zirconium acetate and yttrium nitrate and drying to form a glass which was then heat-treated to decompose the organic constituents and to allow densification of the oxide. Compositions in the range 1 to 5 mole% Y_2O_3 (where grain growth is known to be inhibited) were heat-treated for various periods in the temperature range 1400-1600°C, for which these compositions should lie in a two-phase tetragonal (low Y_2O_3) cubic (high Y_2O_3) region. X-ray, TEM and SEM studies were done to quantify grain growth rates and relate these to microstructural evolution. It has become clear that the partitioning phenomenon in the two-phase region is more complex than thought previously. Measurements of compositional variations (using analytical transmission electron microscopy) within and between grains after various heat-treatment periods indicate that the

partitioning begins with small composition fluctuations between grains rather than by nucleation of grains with the two equilibrium compositions. Phase partitioning was observed to be extremely sluggish, requiring many weeks at normal sintering temperatures to establish equilibrium phases. Moreover, grain growth was observed to be extremely slow during the very early stages of partitioning. Therefore, it appears that a small difference in Y_2O_3 content in adjacent grains serves to inhibit grain boundary movement and hence grain growth. It is known that the lattice parameters of the tetragonal structure vary with Y_2O_3 content. On the basis of these observations we have postulated that movement of a grain boundary separating grains of slightly different composition would generate strain energy because of the lattice parameter mismatch. An analytical model has been developed to account for the inhibiting effect of the strain energy on grain growth. The model predicts rapid growth of the grains to a stable size, consistent with experimental observations, and suggests that the key to similar grain growth control in other two-phase systems lies in selecting alloy systems in which there is a similar variation of lattice parameter with alloying species.

4. An exciting offshoot from the research on the ZrO_2/Y_2O_3 system was the discovery that fibers could be drawn from the acetate precursor at a certain stage during the drying process, and because of the grain growth control achievable in this system, fibers with very high strength were produced after heat treatment. Fibers of composition 2.5 mole% Y_2O_3 were drawn and heat-treated at 1400°C. The fibers had uniform diameters in the range 1 to 5 μm and grain size ≤ 0.2 μm. The strengths of the fibers were measured in direct tension and values as high as 2.6 GPa were obtained. Further optimization of heat-treatment time and temperature might be expected to yield even higher strengths.

5. A new approach for measuring the nature and distribution of transformation strains around a surface-breaking crack was demonstrated. This is important because, although a general understanding exists of the mechanics of crack tip shielding by a transformation zone, and there is a formulation for calculating the toughening quantitatively once the zone shape and transformation strains are specified, there are large gaps in our knowledge of the factors that are critical for designing optimum materials. These include the microstructural characteristics that dictate the zone shape and size, the nature of the transformation strain within the zone (i.e., whether both dilation and shear are present), and the role of continuously variable volume fraction of

transformation across the zone, rather than a step profile. Progress in these areas is presently hindered by lack of knowledge of the critical stress state needed for triggering the transformation and limitations of methods for experimentally measuring these important characteristics of the zone. Our approach involved measuring out-of-plane distortions of the free surface at various locations across the transformation zone adjacent to the crack and comparing the measurements with the distortions calculated by modeling the zone as a set of nested inclusions. A convenient procedure was devised for adjusting the distribution of transformation strains in the inclusions and fitting the calculated profiles to experimentally measured values to allow the strain distribution to be deduced. The Raman microprobe was also used to measure variations of monoclinic and tetragonal phase content within the zone. Good agreement was found between these measurements and the distribution obtained from surface uplift measurements. The degree of transformation was found to be inhomogeneous, being maximum near the crack and decreasing linearly or faster with distance from the crack plane. The results suggested that, over most of the transformation zone, the transformation strains were dilational (i.e., shear component relieved by twinning), but there was also evidence that a significant shear strain persists near the crack plane.

During the final year effort was concentrated on (1) detailed characterization of transformation zones in toughened zirconia, (2) fundamental studies of phase stability (reversibility, low temperature) in Mg-PSZ and (3) fatigue crack growth induced by cyclic loading.

The mechanical properties of high-toughness magnesia-partially stabilized zirconia were found to be dramatically altered by a single cooling cycle between room temperature and -196°C (Section 3). In situ Raman spectroscopy and x-ray diffraction were used to correlate the changes in mechanical properties with structural changes that occur at temperatures below ~ -100°C. Most of the tetragonal precipitates that are responsible for toughening transformed to an orthorhombic phase with unit cell volume intermediate between those of the tetragonal and monoclinic phases. This was a surprising result: an orthorhombic phase has been observed previously, but only in thin TEM foils, where the special relaxed constraint was thought to play a role, and in bulk materials at very high pressures. The orthorhombic phase was stable with heating to 300°C, but transformed back to the tetragonal structure when heated to 400°C. Surprisingly, the orthorhombic phase was not readily transformable by stress, with the

consequence that, after the cooling cycle, most of the high-toughness properties of the original tetragonal-containing material were lost. Moreover this last result implies that the orthorhombic phase is not a necessary intermediate step in the martensitic tetragonal-monoclinic transformation as suggested in some prior studies.

Reversibility of the tetragonal-to-monoclinic transformation was discovered earlier in this program by observing surface distortions caused by varying amounts of transformation in adjacent grains, and confirmed by in situ x-ray diffraction in our laboratory and by TEM observations in other laboratories. Although the surface distortion measurement remains the most sensitive and convenient method for detecting small amounts of transformation, it is complicated by the fact that similar distortion can also be caused by elastic anisotropy. The separate contributions from elastic anisotropy and reversibility were measured and analyzed in Mg-PSZ (Section 4); the two contributions have similar magnitudes and dependence on crystallographic orientation.

The subcritical growth of fatigue cracks in cyclic loading was demonstrated in a series of Mg-PSZ materials with toughnesses ranging from 2 MPa $m^{1/2}$ (no transformation toughening) to 16 MPa $m^{1/2}$ (Section 5). This work was done in collaboration with R. Dauskardt and R. Ritchie at U.C. Berkeley. The crack growth was measured in compact tension specimens. Although the growth rates were accelerated in moist environments, a true, mechanically induced, cyclic contribution was also demonstrated at stress intensity factors as low as 50% of the steady state toughness. This is perhaps the first unequivocal demonstration of true cyclic fatigue in ceramics. Growth rates were dependent upon the stress intensity range (ΔK), the load ratio, and the fracture toughness; the data could be fitted to a power law function of ΔK, with exponent in the range 21 to 42. Moreover, for a given growth rate, ΔK scaled approximately with the steady-state fracture toughness. This result and the observation of transient accelerations and retardations after increasing or decreasing the load amplitude are consistent with the existence of toughening by a zone shielding mechanism, with growth rates being determined by the local crack tip stress intensity factor. Detailed measurements of zone characteristics (Section 6) are also consistent with this conclusion. However, the actual mechanism of fatigue has not been determined.

Transformation zones surrounding cracks in several toughened Mg-PSZ ceramics were characterized by optical interference measurement of surface uplift and

by Raman spectroscopy (Section 6). The results indicate that the degree of transformation is not uniform within the zone, that the frontal zone is approximately defined by a contour of constant hydrostatic stress in the crack tip field, and that transformation of all the tetragonal phase was never observed in regions adjacent to cracks (contrary to TEM observations). The reductions in crack tip stress intensity factor due to shielding from the transformation zone were calculated using the Raman measurements of the zone profile. An assumption that only the dilation component of the transformation strain remained (i.e., shear component relieved by twinning) led to an underestimate of the toughness increase.

2.0 PUBLICATIONS RESULTING FROM PROGRAM AND CONTRIBUTING PERSONNEL

2.1 Publications Resulting from Program

1. "Strength Characteristics of Transformation Toughened Zirconia," by D.B. Marshall, J. Am. Ceram. Soc. 69[3], 173-80 (1986).

2. "Reversible Stress-Induced Martensitic Transformation in ZrO_2," by D.B. Marshall and M.R. James, J. Am. Ceram. Soc. 69[3], 215-217 (1986).

3. "Crack Resistance Curves in Magnesia-Partially-Stabilized Zirconia," by D.B. Marshall and M.V. Swain, J. Am. Ceram. Soc. 71[6], 399-407 (1988).

4. "Transformation Stability in Magnesia-Partially Stabilized Zirconia," by D.B. Marshall to be published in J. Am. Ceram. Soc.

5. "Controlling Grain growth," by F.F. Lange, pp. 497-508 in Ceramic Microstructures '86, Ed J. Pask and A.G. Evans, Plenum (1987).

6. "High Strength Zirconia Fibers," by D.B. Marshall, F.F. Lange and P.E.D. Morgan, J. Am. Ceram. Soc. 70[8], C187-188 (1987).

7. "Controlling Microstructures through Phase Partitioning from Metastable Precursors: The ZrO_2-Y_2O_3 System," by F.F. Lange, D.B. Marshall and J.R. Porter in Proceedings of Ceramic Uitrastructures (1987).

8. "On the Thermoelastic Martensitic Transformation in Tetragonal ZrO_2," by A.H. Heuer, M. Ruhle and D.B. Marshall, to be published in J. Am. Ceram. Soc.

9. "Surface Displacement Analysis of the Transformed Zone in Magnesia Partially Stabilized Zirconia," by B.N. Cox, D.B. Marshall, D. Kouris and T. Mura, J. Eng. Mat. Tech. 110[2], 105-109 (1988).

10. "Structural and Mechanical Property Changes in Toughened Mg-PSZ at Low Temperatures," by D.B. Marshall, M.R. James and J. Porter, J. Am. Ceram. Soc., in press.

11. "Cyclic Fatigue Crack Propagation in Ceramics: Behavior in Overaged and Partially Stabilized MgO-ZrO_2," by R.H. Dauskardt, D.B. Marshall and R.O. Ritchie, Mat. Res. Soc. Proceedings, Symposium on Fracture Mechanics of Structural Ceramics, in press.

12. "Reversible Transformation and Elastic Anisotropy in Mg-PSZ," by D.B. Marshall and M.V. Swain, submitted to J. Am. Ceram. Soc.

13. "Crack Tip Transformation Zones in Toughened Zirconia," by D.B. Marshall and M. Shaw, to be published in J. Am. Ceram. Soc.

14. "Cyclic Fatigue Crack Propagation in MgO-PSZ Ceramics," by R. Dauskardt, D.B. Marshall and R.O. Ritchie, in preparation for J. Am. Ceram. Soc.

2.2 Personnel Involved in Program

The principal investigators were Dr. D.B. Marshall and, for the first year before his departure for U.C. Santa Barbara, Dr. F.F. Lange. Other contributors from the Science Center were Dr. M.R. James, Dr. P.E.D. Morgan, Dr. J.R. Porter, Dr. B.N. Cox, Mr. M. Shaw and Mr. E. Wright. The program also benefitted from several collaborators with universities and other institutions: M.V. Swain from CSIRO, Australia; R.H. Dauskardt and R.O. Ritchie from U.C. Berkeley; and A.H. Heuer and M. Readey from Case Western Reserve University.

3.0 STRUCTURAL AND MECHANICAL PROPERTY CHANGES IN TOUGHENED Mg-PSZ AT LOW TEMPERATURE*

*Accepted for publication in the Journal of the American Ceramic Society.

STRUCTURAL AND MECHANICAL PROPERTY CHANGES IN TOUGHENED Mg-PSZ AT LOW TEMPERATURES

D.B. Marshall, M.R. James and J.R. Porter

Rockwell International Science Center
Thousand Oaks, CA 91360

ABSTRACT

The mechanical properties of high-toughness magnesia-partially stabilized zirconia were found to be dramatically altered by a single cooling cycle between room temperature and -196°C. Raman spectroscopy and x-ray diffraction were used to correlate the changes in mechanical properties with structural changes that occur at temperatures below ~ -100°C. Most of the tetragonal precipitates that are responsible for toughening transformed to an orthorhombic phase with unit cell volume intermediate between those of the tetragonal and monoclinic phases. The orthorhombic phase was stable with heating to 300°C, but it transformed back to the tetragonal structure when heated to 400°C. Surprisingly, the orthorhombic phase was not readily transformable by stress, with the consequence that, after the cooling cycle, most of the high-toughness properties of the original tetragonal-containing material were lost.

1. INTRODUCTION

Zirconia-containing ceramics can be toughened dramatically by the martensitic tetragonal-to-monoclinic transformation in localized zones around cracks.[1-13] However, high toughening requires a very narrow range of microstructures in which ZrO_2 grains or precipitates are on the verge of spontaneous transformation. Since the transformability of constrained ZrO_2 particles is sensitive to the degree of undercooling from the unconstrained M_s (martensitic start) temperature, both the degree of toughening and the stability of the microstructure are expected to be very sensitive to temperature changes.

The highest toughness ZrO_2 ceramics are from the magnesia-partially stabilized zirconia system (Mg-PSZ).[9-15] In optimally aged materials, with toughness up to 18 $MPa \cdot m^{1/2}$, the tetragonal precipitates are so close to spontaneous transformation at room temperature that a fraction do transform during cooling, and others begin to transform under applied tensile stresses as low as 300 MPa.[10,11] The purpose of this paper is to examine whether cooling below room temperature causes further transformation of these precipitates, and thereby a loss of toughening at cryogenic temperatures, or even more importantly, degradation of room-temperature mechanical properties after a single cooling cycle. Swain[16,17] has shown previously that the fracture toughness of such materials is reduced at temperatures below about -100°C, and that thermal expansion measurements indicate a volume increase in the temperature range -80 to -100°C. Moreover, the tetragonal-to-monoclinic transformation after cooling in liquid nitrogen has been inferred from x-ray measurements in several Mg-PSZ ceramics,[18] although the measured phase differences in that work approached the limits of experimental error. We will show that cooling does indeed cause a transformation, but that the transformation product is not the monoclinic structure. Instead, it is an orthorhombic phase of ZrO_2.

2. EXPERIMENTAL

The material of primary interest in this study is a high-toughness, 9 mole% MgO-partially stabilized zirconia (Mg-PSZ), which was fabricated by sintering at 1700°C, with controlled cooling to room temperature, followed by subeutectoid heat treatment at 1100°C. Specimens that had been given several different heat treatments to produce various degrees of transformation toughening were examined (Table 1). These materials contained lens-shaped, MgO-depleted precipitates, ~ 200 nm in diameter, in a fully stabilized (MgO-rich) cubic matrix. In the high-toughness material, most of the precipitates were of the tetragonal structure, but some (~ 13 vol%) had transformed to the monoclinic phase during cooling. Some of this material was overaged by heating to 1400°C for two days, resulting in transformation of all precipitates to monoclinic structure upon cooling. Two other Mg-ZrO_2 ceramics, with different compositions and heat treatments, were also tested for comparison: a 14 mole% MgO-ZrO_2 which was all stabilized cubic phase, and a 3 mole% MgO-PSZ which contained tetragonal precipitates that cannot be transformed to monoclinic phase by applied stress.

The room-temperature mechanical properties of the 9 mole% MgO materials were reported in detail elsewhere.[19] In tensile loading of specimens of the high-toughness material with polished surfaces, the stress-strain response was nonlinear because of stress-induced transformation and microcracking at stresses above ~ 300 MPa. The sequence of damage development is shown in Fig. 1. Stresses below 300 MPa caused reversible surface roughening, which was correlated with tetragonal-to-monoclinic transformation, whereas higher stresses resulted in permanent transformation and the formation and stable growth of microcracks to lengths up to 1 mm. The stable crack growth was attributed to a resistance curve (R curve) that increased with crack extension. The

steady-state fracture toughness was ~ 13 MPa•$m^{1/2}$, and transformation zones ~ 100 μm in width around cracks were readily observed because of surface uplift due to transformation strains (Fig. 1b). The material with 9 h heat treatment had a steady-state fracture toughness of ~ 9 MPa•$m^{1/2}$ and also exhibited nonlinear stress-strain response, R-curve behavior and transformation zones around cracks, but all less extensive than in the 24 h heat-treated material. The material that was not heat treated at 1100°C did not show nonlinear load-deflection response or stable microcrack growth during failure testing, but a small transformation zone was observed around the crack that caused failure. Transformation zones were not detected around cracks in the 3 and 14 mole% MgO-ZrO_2 materials.

Structural changes occurring during cooling to -196°C were monitored in-situ for some materials by optical microscopy and Raman spectroscopy, using a small cooling stage with a quartz window. Optical microscopy was done with both Nomarski interference and conventional interference methods to allow detection and measurement of surface distortions produced by transformation strains. Raman spectroscopy was done using a microprobe with a spot size of ~ 20 μm when the specimen was in the cooling stage and ~ 1 to 2 μm otherwise.

X-ray diffraction was done at room temperature, using Cu or Cr radiation and a liquid-nitrogen-cooled energy-dispersive detector. Step scanning was used with counting times ~ 20 h over the range 2θ = 10-90° and with 5000 counts accumulated at each 0.05° step. Diffraction peak positions and peak half-breadths were obtained by fitting the profiles to Pearson VII functions after background subtraction. Angles were calibrated using a silicon standard.

3. RESULTS

3.1 Optical Observations

The polished surface of a peak toughness Mg-PSZ after cooling in liquid N_2 is shown in Fig. 2. Surface distortions similar to those produced by stress-induced tetragonal-to-monoclinic transformation (Fig. 1) are evident in the Nomarski interference micrograph. Quantitative measurements using conventional interference microscopy indicated that the amplitude of the distortion (~ 50 nm) was larger than that due to the reversible transformation at low applied stresses (~ 20 nm) (Fig. 1(a)), but smaller than that due to permanent transformation (~ 100 to 200 nm) (Fig. 1(b)).

The stress-induced transformation caused relatively uniform uplift of areas that span several grains (presumably, those grains most favorably oriented relative to the applied stress), whereas cooling to liquid N_2 caused general uplift of most of the surface except for isolated areas ~ 20 μm diameter. The areas of surface depression were found to correspond to regions, usually near the centers of grains, that contained comparatively large precipitates which transformed to monoclinic structure during cooling (Fig. 2b). Formation of these large precipitate regions has been discussed by Hughan and Hannink.[20]

During in-situ experiments using the cooling stage, the distortions in Fig. 2 were found to develop over the temperature range -80°C to -120°C and then remain unchanged as the temperature was lowered to -196°C and increased to +96°C. Subsequent heating in a separate furnace for 10 min at 300°C also left the surface distortion unaltered. However, after 3 min at 400°C, most of the distortions disappeared. The temperature range over which surface uplift developed coincides with the temperature range

over which Swain[17] previously observed a volume increase from thermal expansion measurements. The persistence of the volume expansion upon heating to room temperature is also consistent with Swain's results.

Similar response was observed in the intermediate toughness Mg-PSZ, but the surface distortions appeared at lower temperatures (-120°C to -160°C), again consistent with Swain's thermal expansion measurements. Comparison of polished surfaces of the other materials in Table 1 did not reveal any surface distortions.

3.2 Raman Spectroscopy

Raman spectra from the high-toughness Mg-PSZ before and after immersion in liquid N_2 are shown in Fig. 3. Also shown for comparison are spectra from 14% Mg-ZrO_2 (cubic structure) and the overaged PSZ (cubic matrix with monoclinic precipitates). The spectrum obtained after cooling to -196°C contains at least eleven peaks in the range 100-700 cm^{-1} that were not present before cooling, and the original tetragonal peaks are all present, but greatly reduced in intensity. Two of the new peaks (338 and 480 cm^{-1}) coincide with peaks of the monoclinic phase (Fig. 3(c)), but the remaining nine do not belong to any of the tetragonal, monoclinic or cubic phases. Moreover, there are several strong peaks in the monoclinic spectrum of Fig. 3(c) that do not appear in Fig. 3(b) (e.g., 177, 384 cm^{-1}). Therefore, cooling to -190°C caused transformation of most of the tetragonal precipitates to a phase that does not have the monoclinic symmetry.

Results from in-situ Raman measurements during cooling of the high-toughness Mg-PSZ are shown in Fig. 4. The transformation occurred over the temperature range -80 to -120°C, corresponding to the temperature range over which volume expansions and surface roughening were observed. Moreover, after the heat treatment at 400°C, when

the surface distortions disappeared, the Raman spectrum returned to the same as before cooling (Fig. 5). In-situ measurements from the intermediate toughness Mg-PSZ yielded similar results, with the transformation occurring over the range -120°C to -160°C, again consistent with the surface roughening and thermal expansion results. Raman measurements from the other materials in Table I did not reveal any changes in the spectra before and after immersion in liquid N_2.

3.3 X-Ray Measurements

X-ray diffraction patterns obtained at room temperature for the high-toughness material before and after cooling in liquid N_2 are compared in Fig. 6. The specimen was located in the same position and orientation for both x-ray scans. Before cooling, the material contained ~ 13% monoclinic precipitates, ~ 30% tetragonal precipitates and the remainder cubic matrix. After cooling, there was no change in the intensities of the monoclinic peaks (e.g. $(11\bar{1})$ and (111)) and very little change in the superimposed cubic-tetragonal peaks. However, the tetragonal peaks that were separated from the cubic peaks (i.e., (002), (022), (113) and (004)) almost disappeared, and many new peaks appeared (shaded in Fig. 6 and listed in Table 2).

All of the new reflections could be accounted for by indexing a tetragonal (or orthorhombic) unit cell with dimensions a = b = 0.5073 nm and c = 0.5260 nm. The comparisons between observed and calculated d-spacings are shown in Table 2. Also shown in Table 2 are the calculated positions of reflections that overlapped with cubic peaks and reflections that were missing, but which if present would not overlap with cubic peaks. The optimum cell dimensions were obtained using a cell-fitting routine with observed reflections that did not overlap with cubic peaks. The cell-fitting routine was constrained to a unit cell with a = b, because none of the reflections that would split for

a ≠ b were observed to do so. Two further approaches were taken to determine whether a difference between a and b could be resolved. In one, Cr radiation was used to measure the (310)/(130) peak at higher resolution; a single peak was obtained and an upper bound for the difference between a and b was estimated to be 0.0005 nm. The second approach was to plot the peak half-widths (determined by fitting Pearson VII functions to the profiles) as a function of 2θ: peak broadening should exist for reflections of the type (hkl), (khl) if a ≠ b, whereas reflections of the type (hhl) would not be broadened. However, a significant difference between the peak widths of these two types of reflection was not observed. This result also placed an upper bound of approximately 0.0005 nm on the difference between a and b.

The absence of any restrictions on the allowed non-zero (hkl) indicates that the lattice is primitive, with either tetragonal or orthorhombic space groups. The missing reflections of the type (odd, odd, zero) indicate the existence of a glide plane, a/2 and/or b/2 on (001). However, a tetragonal space group would require both of these glide directions, which would restrict the allowed (hko) reflections to those with both h and k even. Therefore, the existence of the (230)/(320) reflection eliminates the tetragonal space group. Analysis of the other allowed reflections (i.e., (011) and (013) present, (001) and (003) missing) indicates either a glide plane c/2 on (100) with mirror plane (010), or a glide plane c/2 on (010) with mirror plane (100). Therefore, the possible space groups relative to the above axes are Pmca, Pcma, Pcmb, or Pmcb. Rotation of the axes converts each of these to one of the standard forms Pbcm or Pbam. These two space groups cannot be distinguished using our data.

Close examination of the x-ray diffraction patterns revealed that the orthorhombic phase was present in the as-received material in very small quantities which may normally go unnoticed. An enlargement of the region around the (113) peaks is

shown in Fig. 6(c): peaks of similar relative size, just above the limit of detection, were identified in the as-received material for all of the other orthorhombic reflections. From the relative peak areas, the initial volume fraction of orthorhombic phase is estimated to be ≤ 2%. Similarly, the amount of residual tetragonal phase remaining after cooling in liquid N_2 was estimated to be ~ 6 vol%.

3.4 Mechanical Properties

The steady-state fracture toughness of the high-toughness Mg-PSZ was recently measured[16] at -196°C and found to be reduced from ~ 13 MPa•$m^{1/2}$ at room temperature to ≈ 7 MPa•$m^{1/2}$. This toughness is higher than that of the overaged material (3 MPa•$m^{1/2}$, Table 1), indicating that, although the degree of transformation toughening was reduced at -196°C, toughening was not completely eliminated. The steady-state toughness is similar to that of the low-toughness Mg-PSZ (Table 1) that was not given the subeutectoid heat treatment.

3.4.1 Flexural Loading

Flexural loading of the high-toughness Mg-PSZ after cooling to -196°C and warming to room temperature resulted in linear stress-strain curve to failure and strength of 520 MPa. There was no permanent transformation or stable microcrack growth during loading, although in one experiment a microcrack ~ 50 μm in length initiated and was stable for ~ 2 seconds at constant load before extending unstably. Post-failure examination of the surface that was stressed in tension revealed surface uplift, indicative of the presence of a transformation zone, around the crack that caused failure, and around several cracks that branched from the main one (Fig. 7(a)). However, the width of the transformation zone was substantially smaller (~ 10 μm) than in the specimen

which had not been cooled to -196°C (100 μm). The transformation zone width was about the same as in the low-toughness Mg-PSZ that was not heat treated at 1100°C, implying that the steady-state toughness is ≈ 6 MPa•$m^{1/2}$ and therefore similar to the toughness measured at -196°C.

After heating to 400°C for 3 min, mechanical behavior that is characteristic of the high-toughness Mg-PSZ was restored. During loading, permanent transformation developed and stable microcracks grew to ~ 1 mm before failure. The stress-strain curve was nonlinear, with the apparent flexural strength of 600 MPa and a true failure stress of 400 MPa.* Stable microcracks and permanent transformation, as well as a larger transformation zone around the main crack, are evident in the post-failure micrograph of Fig. 7(b).

3.4.2 Indentation Experiments

Indentations (300 N Vickers) made in the high-toughness Mg-PSZ before and after cooling to -196°C and after heating to 400°C are compared in Fig. 8(a-f). Cooling of the high-toughness material containing an indentation (Fig. 8(b) caused surface distortions as in Fig. 2(b) remote from the indentation, but did not change the surface distortions associated with the tetragonal-monoclinic transformation around the indentation (compare Figs. 8(c) and (d)). These surface distortions around the indentation are also much larger than those due to the tetragonal-orthorhombic transformation, consistent with the observations in Section 3.1. Indentation after a cooling cycle to -196°C and back to room temperature induced a much smaller area of tetragonal-monoclinic trans-

* For Mg-PSZ with nonlinear stress-strain response in tension, the stress-strain curve in compression is linear, with the result that the apparent flexural stress calculated from beam theory is larger than the actual stress on the tensile surface.[11]

formation (Fig. 8(e)), similar in size to that in the low-toughness Mg-PSZ.[19] Indentation after subsequent heating to 400°C and cooling to room temperature (Fig. 8(f)) resulted in a transformation zone similar in size to that in the original material. These results indicate that the propensity for stress-induced transformation decreases upon cooling to -196°C and is restored by heating to 400°C, consistent with the results obtained in flexural loading.

4.0 DISCUSSION

The results of the previous section have directly linked the formation of an orthorhombic phase of ZrO_2 to dramatic changes in mechanical properties of high-toughness Mg-PSZ. A single cooling cycle from room temperature to -100°C results in transformation of tetragonal precipitates to the orthorhombic phase, with an accompanying reduction in fracture toughness and elimination of both nonlinear stress-strain response and R-curve behavior. However, the original high-toughness properties can be restored by a subsequent heating cycle to 400°C, which causes transformation of the orthorhombic phase back to the tetragonal structure.

Orthorhombic phases of ZrO_2 have been observed by transmission electron microscopy (TEM) in thin foils of all of the transformation-toughened ZrO_2 ceramics.[21-23] A high-pressure orthorhombic phase has also been observed in ZrO_2, both at high pressure[24,25] and at atmospheric pressure after quenching from high pressure and temperature[26,27] (although a high pressure modified tetragonal structure has also been proposed[28]). In both the thin foil and the high-pressure studies, the space group Pbcm was assigned; this is one of the two possible space groups for the present low-temperature orthorhombic phase. Moreover, there are some similarities (but also some significant differences) in the cell parameters (Table 3); the a and b dimensions for the orthor-

hombic phase in thin foils of Mg-PSZ are close to the values for the low-temperature phase, but c is smaller, whereas the largest dimension for the high-pressure phase (c = 0.5257) is close to that of the low-temperature phase, but a and b differ. Raman spectra have also been obtained for the high-pressure phase, both at high pressure using a diamond anvil cell[24,28] and at atmospheric pressure in materials with quenched high-pressure phase.[27] These spectra differ from that of the low-temperature phase (Fig. 3). However, the total number of peaks is similar, consistent with the space group determinations.

The tetragonal-orthorhombic transformation in the present experiments is accompanied by an increase in unit cell volume of 1.1% (unit cell dimensions listed in Table 3), which is about a quarter of the volume increase accompanying the tetragonal-to-monoclinic transformation. Combined with the measured volume fraction of transformation (~ 30%), this implies a total volume change of 0.4% upon cooling the material through the phase transformation. This agrees well with the thermal expansion data of Swain,[17] who measured 0.13% linear expansion when cooling similar material through the temperature range -70°C to -160°C. It is also consistent with the magnitude of the surface distortion observed after cooling (Fig. 2). The surface distortions are associated with regions ~ 20 μm diameter which were monoclinic phase and did not transform during cooling. A volume strain of 0.4% in a region of this size would correspond to linear expansion of 30 nm which is reasonably close to the measured depression depth of ~ 50 nm.

The present experiments are the first to have identified the formation of an orthorhombic phase in bulk material at atmospheric pressure. In the TEM foils, the transformation occurred at atmospheric pressure, but it was observed only in the thinnest regions (i.e., thickness < precipitate diameter), thus leading to the suggestion that it was

an artifact of the special constraint configuration of the thin foil and the foil preparation techniques. In support of this suggestion, Muddle and Hannink[23] showed directly that ion beam thinning can induce the tetragonal-orthorhombic transformation. The transformation in the present experiments is believed to occur throughout the bulk rather than only at free surfaces for the following reasons: 1) the bulk volume change calculated above on the basis of the measured unit cell parameters agrees with bulk expansion measurements; and 2) the penetration depths for the x-ray measurements were ~ 10 μm, and the amount of orthorhombic phase detected by Raman spectroscopy was the same using either high or low magnification lens systems that collect from depths ~ 2 μm and ~ 20 μm, respectively. For these depths, which are up to two orders of magnitude larger than the precipitate size, the effect of the free surface on the elastic strain energy associated with a transformation is negligible.

The stability of the orthorhombic phase determines its influence on mechanical properties of the ceramic. In both TEM foils and quenched high-pressure materials, the stress-induced orthorhombic-to-monoclinic transformation occurred readily (in the TEM foils by stresses caused by thermal cycling of adjacent regions with the electron beam,[22,23] and in the quenched material by grinding in a mortar[26]). In contrast, the low-temperature orthorhombic phase appears to be very resistant to stress-induced transformation to monoclinic structure, as reflected in the changes in room-temperature mechanical properties after cooling in liquid N_2. Moreover, the orthorhombic-to-monoclinic transformation could not be detected by Raman spectroscopy on surfaces that had been ground after the cooling cycle to -196°C. Since the tetragonal phase in this material transforms very readily to the monoclinic structure, the formation of the orthorhombic phase cannot be an essential intermediate step in the tetragonal-monoclinic transformation.

There is, however, some indirect evidence to suggest that the orthorhombic-to-monoclinic transformation can occur at high stresses. After cooling in liquid N_2, the degree of toughening is reduced, but toughening is not eliminated altogether, and small transformation zones adjacent to cracks are evident. These zones could arise from transformation of either the orthorhombic precipitates or the small fraction of tetragonal precipitates that survive the cooling cycle. Since transformation during cooling occurs only in the two Mg-PSZ materials that exhibit high toughness, it may be argued that the precipitates that transform to the new phase during cooling are the same ones that are most easily transformed by stress, and which give rise to the large toughening. Raman measurements from regions adjacent to cracks in the high-toughness Mg-PSZ indicate that only some of the tetragonal precipitates (approximately half) transform to monoclinic structure. Moreover, the fraction of tetragonal phase remaining in the crack tip zone is larger than the fraction remaining after cooling to 196°C (compare Figs. 3(b) and 9). These results imply that all of the tetragonal precipitates remaining after cooling should also remain untransformed in the crack tip zone, and therefore that the crack tip transformation zone arises from the stress-induced orthorhombic-to-monoclinic transformation.

An attempt was made to identify the source of residual toughening after cooling to -196°C by comparing Raman spectra from areas adjacent to, and remote from, the crack that caused failure in flexural loading (Fig. 10). An increase in the signal from the monoclinic phase is evident (shaded peaks) confirming that it is indeed transformation to the monoclinic phase that gives rise to the transformation zone. However, the sensitivity is not sufficiently high to determine whether this transformation corresponded to a decrease in tetragonal or orthorhombic phase.

5. CONCLUSIONS

A single cooling cycle for high-toughness Mg-PSZ to temperature below ~ -100°C causes severe degradation of room-temperature mechanical properties. The fracture toughness is reduced from ~ 13 $MPa \cdot m^{1/2}$ to ~ 6 $MPa \cdot m^{1/2}$, the tensile stress-strain response becomes linear up to failure instead of being nonlinear, and the R-curve characteristic of high-toughness Mg-PSZ is lost. However, the original high-toughness properties are restored by heating to 400°C.

The degradation in mechanical properties coincides with the transformation of most of the tetragonal precipitates to an orthorhombic phase with unit cell volume between those of the tetragonal and monoclinic phases. The orthorhombic phase is stable upon heating to at least 300°C, but at 400°C (for 3 min), it transforms back to the tetragonal structure. Traces of the orthorhombic phase were also detected in the as-received material that had not been cooled below room temperature.

ACKNOWLEDGEMENTS

Funding for this work was supplied by the Air Force Office of Scientific Research under Contract No. F49620-85-C-0143. Some of the materials studied were kindly suppied by M.V. Swain. The authors are grateful to P.E.D. Morgan for use of a cell-fitting routine to optimize the cell dimensions, and to K.T. Miller for collecting some of the in-situ Raman data.

REFERENCES

1. R.S. Garvie, R.H.J. Hannink and R.T. Pascoe, "Ceramic Steel?," Nature 258 (5537), 703-704 (1975).

2. D.L. Porter and A.H. Heuer, "Mechanisms of Toughening Partially Stabilized Zirconia," J. Am. Ceram. Soc. 60 (3-4), 183-84 (1977).

3. F.F. Lange, "Transformation Toughening: Part 5. Effect of Temperature and Alloy on Fracture Toughness," J. Mat. Sci. 17, 255-263 (1982).

4. F.F. Lange, "Transformation Toughening: Part 4. Fabrication, Fracture Toughness and Strength of Al_2O_3-ZrO_2 Composites," J. Mat. Sci. 17, 247-54 (1982).

5. N. Claussen and M. Ruhle, "Design of Transformation Toughened Ceramics," pp. 137-63 in Advances in Ceramics, Vol. 3, Ed., A.H. Heuer and L.W. Hobbs, Am. Ceram. Soc. (1981).

6. M.V. Swain, R.H.J. Hannink and R.C. Garvie, pp. 339-54 in Fracture Mechanics of Ceramics, Vol. 6, edited by R.C. Bradt, A.G. Evans, D.P.H. Hasselman and F.F. Lange, Plenum, NY (1983).

7. R.H.J. Hannink, "Growth Morphology of the Tetragonal Phase in Partially Stabilized Zirconia," J. Mat. Sci. 13, 2487-96 (1978).

8. R.H.J. Hannink, K.A. Johnston, R.T. Pascoe and R.C. Garvie, pp. 116-136 in Advances in Ceramics, Vol. 3, edited by A.H. Heuer and L.W. Hobbs, Am. Ceram. Soc. (1981).

9. M.V. Swain and R.H.J. Hannink, "R-Curve Behavior in Zirconia Ceramics," in Science and Technology of Zirconia II, Advances in Ceramics, Vol. 12, eds., N. Claussen, M. Ruhle and A.H. Heuer, Am. Ceram. Soc., Columbus (1984), pp. 225-239.

10. M.V. Swain, "Inelastic Deformation of Mg-PSZ and Its Significance for Strength-Toughness Relationships of Zirconia Toughened Ceramics," Acta. Met. 33 (11), 2083-91 (1985).

11. D.B. Marshall, "Strength Characteristics of Transformation-Toughened Zirconia," J. Am. Ceram. Soc. 69 (3), 173-180 (1986).

12. R.H.J. Hannink and M.V. Swain, "Magnesia-Partially Stabilized Zirconia: The Influence of Heat Treatment on Thermomechanical Properties," J. Aust. Ceram. Soc. 18 (2), 53-62 (1982).

13. M.J. Ready and A.H. Heuer, "Crack Development in Transformation-Toughened Mg-PSZ," in Advanced Structural Ceramics, Proc. MRS Fall Meeting, Boston (1986).

14. M.J. Ready and A.H. Heuer, "On the Annealing of Test Specimens of High Toughness Mg-PSZ," J. Am. Ceram. Soc. 71 (1), C2-6 (1988).

15. A.H. Heuer, M.J. Ready and R. Steinbrech, "Resistance Curve Behavior of Supertough MgO Partially Stabilized ZrO_2 (Mg-PSZ)," J. Mat. Sci., in press.

16. S. Veitch, M. Marmach and M.V. Swain, "Strength and Toughness of Mg-PSZ and Y-TZP Materials at Cryogenic Temperatures," in Advanced Structural Ceramics, Proc. MRS Fall Meeting, Boston (1986).

17. M.V. Swain, private communication.

18. J.A. Excell and M. Marmach, "Reversible Cryogenically Induced Tetragonal to Monoclinic Phase Transformation in Mg-PSZ," Am. Ceram. Bull. 65 (10) 1404-7 (1986).

19. D.B. Marshall and M.V. Swain, "Crack Resistance Curves in Magnesia-Partially-Stabilized Zirconia," J. Am. Ceram. Soc. 71 (6), 399-407 (1988).

20. R.R. Hughan and R.H.J. Hannink, "Precipitation During Controlled Cooling of Magnesia-Partially-Stabilized Zirconia," J. Am. Ceram. Soc. 69 (7), 556-63 (1986).

21. A.H. Heuer, L.H. Schoenlein and S. Farmer, "New Microstructural Features in Magnesia-Partially-Stabilized Zirconia (Mg-PSZ)," in Science of Ceramics 12, Ed., P. Vincenzini, Cermurgica, Italy, pp. 257-266, 1984.

22. A.H. Heuer, V. Lauteri, S.C. Farmer, R. Chaim, R.-R. Lee, B.W. Kibble and R.M. Dickerson, "On the Orthorhombic Phase in ZrO_2-Based Alloys," J. Mat. Sci., in press.

23. B.C. Muddle and R.H.J. Hannink, "Phase Transformation Involving an Orthorhombic Phase in MgO-PSZ," in Science and Technology of Zirconia, in press.

24. A. Arashi and M. Ishigame, "Raman Spectroscopic Studies of the Polymorphism in ZrO_2 at High Pressures," Phys. Stat. Sol. (a) 71, 313-321 (1982).

25. Y. Kudoh, H. Takeda and H. Arashi, "In-Situ Determination of Crystal Structure for High Pressure Phase of ZrO_2 using a Diamond Anvil and Single Crystal X-Ray Diffraction Method," Phys. Chem. Mineral 3, 233-37 (1986).

26. R. Suyama, T. Ashida and S. Kume, "Synthesis of the Orthorhombic Phase of ZrO_2," J. Am. Ceram. Soc. 68 (12), C314-15 (1985).

27. O. Ohtaka, S. Kume, T. Awami and K. Urabe, "Synthesis of Orthorhombic Phase of $2Y \cdot ZrO_2$," J. Am. Ceram. Soc. 71 (3), C164-66 (1988).

28. B. Alzyab, C.H. Perry and R.P. Ingel, "High Pressure Phase Transitions in Zirconia and Yttria-Doped Zirconia," J. Am. Ceram. Soc. 70 (10), 760-65 (1987).

Table 1

Materials Tested

Material	Heat treatment 1100°C	Heat treatment 1400°C	Steady-State Toughness (MPa•m$^{1/2}$)	Apparent Flexural Strength (MPa)§	True Strength (MPa)
High Toughness[a]	24 h		13	620	400
High Toughness[b]	By manufacturer[b]		13	620	400
Intermediate[a] Toughness	7 h		10	700	600
Low Toughness[a]	0		6	540	540
Overaged[b]		48 h	3		

a. Specimens supplied by M.V. Swain
b. Nilcra
§ Calculated from elastic beam theory; larger than true strength for material with nonlinear stress-strain response in tensile loading.[11]

Table 2

Comparison of Observed and Calculated d Values for Orthorhombic ZrO_2: a = b = 0.5073 nm, c = 0.5260 nm

hkl§		d (nm)	
Overlap with Cubic Reflections	Not Overlapping With Cubic Reclections	Measured	Calculated
	(001)	**	0.5260
	(010)	0.506	0.5073
	(011)	0.3654	0.3651
	(110)	**	0.3587
(111)			0.2964
	(002)	0.2634	0.2630
(020)			0.2536
	(012)	0.2338	0.2335
	(021)		0.2285
	(120)	0.227	0.2269
	(112)	0.2120	0.2121
	(121)	0.2083	0.2083
	(022)	0.1824	0.1826
(220)			0.1793
	(003)	**	0.1753
	(122)	0.1718	0.1718
	(221)	*	0.1697
	(030)	*	0.1691
	(013)	0.1657	0.1657
	(031)	**	0.1610
	(130)	**	0.1604
	(113)	0.1575	0.1575
(131)			0.1534
(222)			0.1482
	(023)	*	0.1442
	(032)	0.1422	0.1422
	(230)	0.1407	0.1407
	(123)	0.1387	0.1387
	(132)	*	0.1369
	(231)	*	0.1359
	(004)	0.1314	0.1315
(040)			0.1268

* Orthorhombic peak not detected but calculated position overlaps with monoclinic peaks.

** Peak not detected and calculated position does not overlap with any preexisting peaks in the as-received material.

§ (hkl) is understood to mean (hkl) and/or (khl).

Table 3

Comparison of Lattice Parameters of Orthorhombic and Tetragonal Phases of Zirconia (nm)*

	a	b	c
Low Temperature (Mg-PSZ) Ortho	0.5073	0.5073	0.5260
TEM Foil (Mg-PSZ) Ortho[a]	0.5088	0.5071	0.5184[a]
[b]	0.508	0.508	0.518[b]
High Pressure (ZrO_2 and Y_2O_3-ZrO_2) Ortho[c]	0.5042	0.5092	0.5257[c]
Tetragonal Mg-PSZ[a]	0.5080		0.5190

a Data from Hannink[28]

b Data from Heuer et al[22]

c Data from Suyama et al[26]

* Note that in this table cell dimensions have been chosen with a < b < c. To express the space group of the orthorhombic phases in the standard form, Pbcm, it is necessary to rotate the axes so that b is the largest.

FIGURE CAPTIONS

Fig. 1 Nomarski interference micrographs of polished surface of high-toughness Mg-PSZ: (a) during loading with tensile stress 300 MPa; (b) stress increased to 380 MPa.

Fig. 2 (a) Polished surface of high-toughness Mg-PSZ after cooling to -196°C. Nomarski interference micrograph. (b) Scanning electron micrograph showing large precipitates within a region of surface depression in (a).

Fig. 3 Raman spectra (room temperature) from high-toughness Mg-PSZ (polished surface) before and after cooling to -196°C, overaged Mg-PSZ (monoclinic and cubic phases), and 14% Mg-PSZ (fully stabilized cubic phase).

Fig. 4 In-situ Raman spectra from high-toughness Mg-PSZ during cooling.

Fig. 5 Raman spectra from high-toughness Mg-PSZ after cooling to -196°C, then heating to 400°C and cooling to room temperature.

Fig. 6 X-ray diffraction patterns (Cu K-α) from high-toughness Mg-PSZ before (a) and after (b) cooling to -196°C. Peaks that appeared after cooling are shaded: (c) to (e) enlargements from regions of (a) and (b).

Fig. 7 Nomarski interference micrographs from tensile surfaces of bars of high-toughness Mg-PSZ that were broken in flexure after: (a) being cooled to -196°C, warmed to room temperature and polished; (b) being cooled to -196°C, heated to 400°C for 3 min, cooled to room temperature and polished.

Fig. 8 (a-f) Vickers indentations (300 N load) in high-toughness Mg-PSZ (Nomarski interference micrographs)

(a) As-received, surface polished before indentations; width of field 1.65 mm.

(b) Same indentation as (a) after cooling to -196°C.

(c) Higher magnification of (a) (note that contrast due to Nomarski interference is lower with this higher power objective lens). Width of field in (c)-(h); 825 μm.

(d) Higher magnification of (b).

(e) Indentation made in another area of the specimen used for (a)-(d), but after cooling to -196°C and warming to room temperature.

(f) Indentation made after cooling to -196°C, heating to 400°C, and cooling to room temperature.

Fig. 9 Raman spectrum from region adjacent to crack in high-toughness Mg-PSZ.

Fig. 10 Raman spectra from regions adjacent to and remote from the crack in Fig. 7(a) (high-toughness Mg-PSZ cooled to -196°C, polished, then broken in flexure). Shaded areas represent monoclinic peaks from area adjacent to crack.

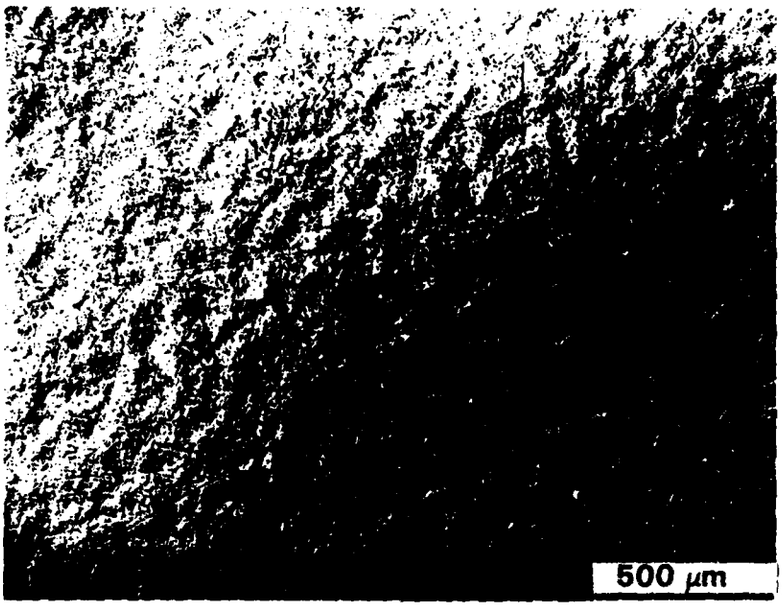

(A)

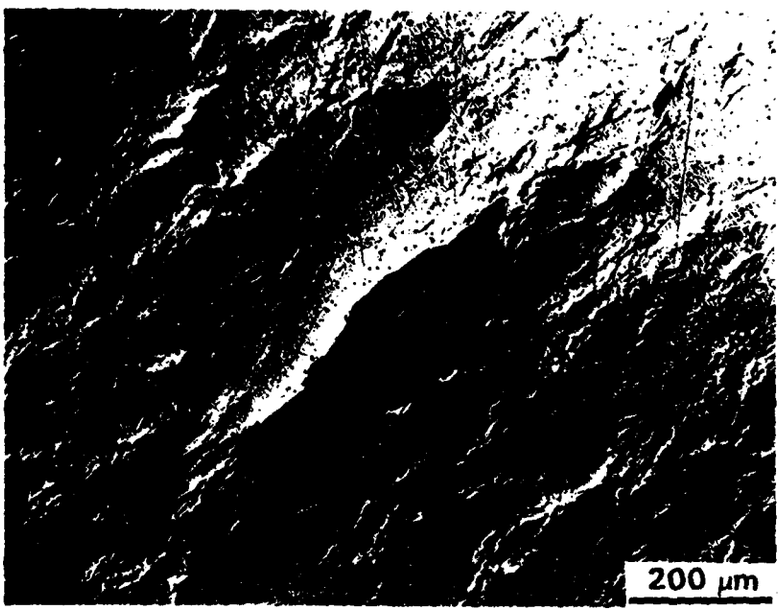

(B)

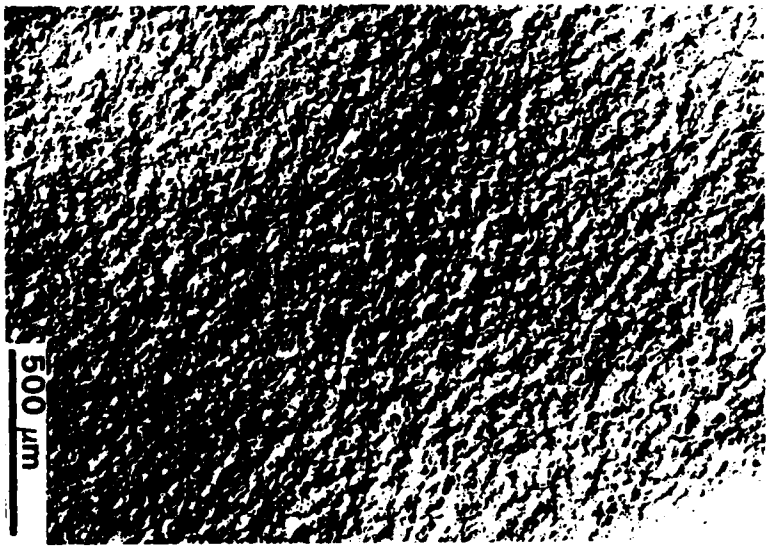
500 μm


3 μm

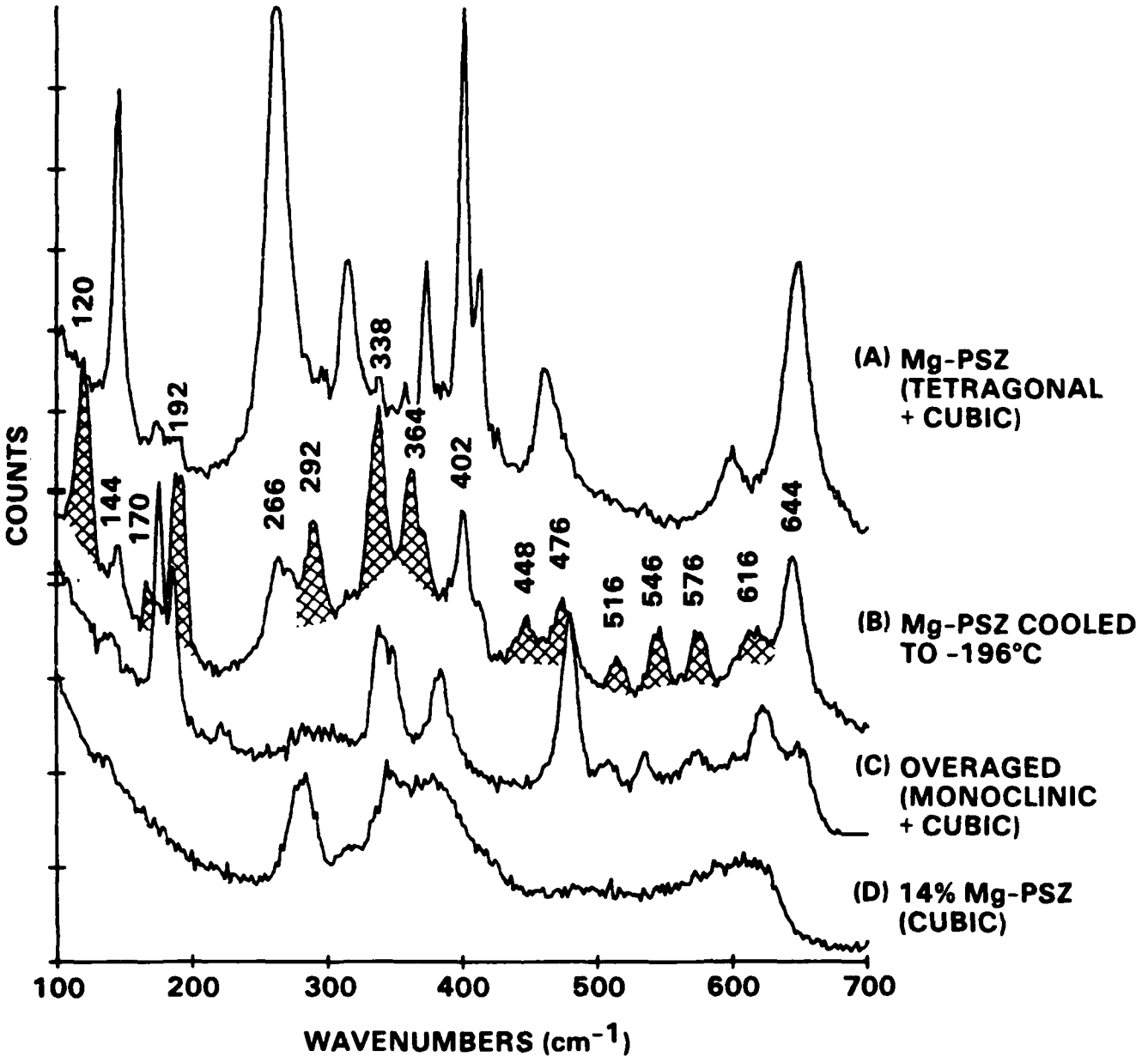
120
144
170
192
266
292
338
364
402
448
476
516
546
576
616
644
COUNTS
(A) Mg-PSZ (TETRAGONAL + CUBIC)
(B) Mg-PSZ COOLED TO -196°C
(C) OVERAGED (MONOCLINIC + CUBIC)
(D) 14% Mg-PSZ (CUBIC)
100
200
300
400
500
600
700
WAVENUMBERS (cm^{-1})

SC5444.FR

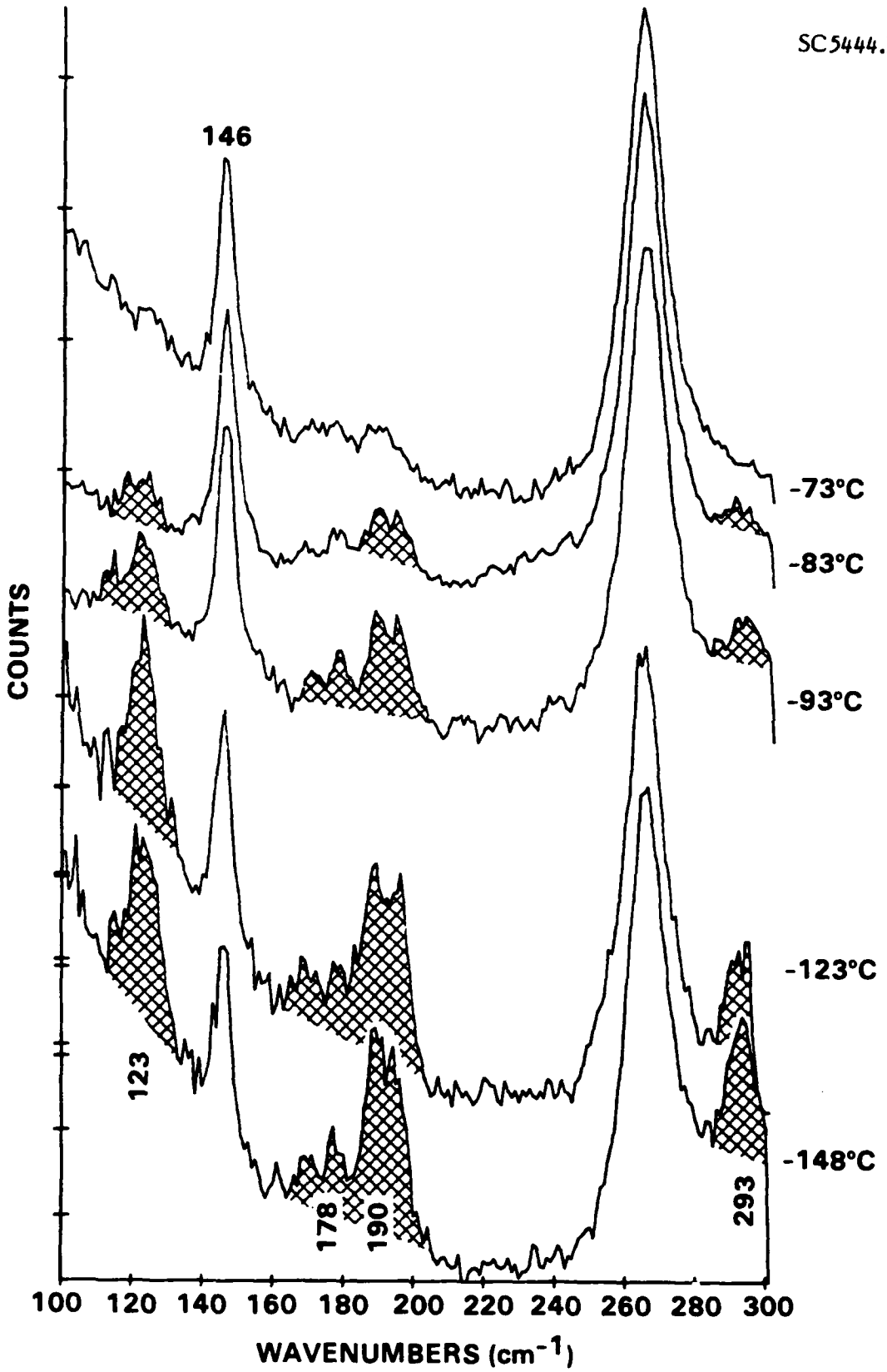

Figure 4

Rockwell International
Science Center
SC5444.FR
SC42497
COOL TO -196°C
HEAT TO 400°C
644
614
576
546
514
476
448
398
362
338
292
266
190
144
122
COUNTS
100
200
300
400
500
600
WAVENUMBERS (cm^{-1})

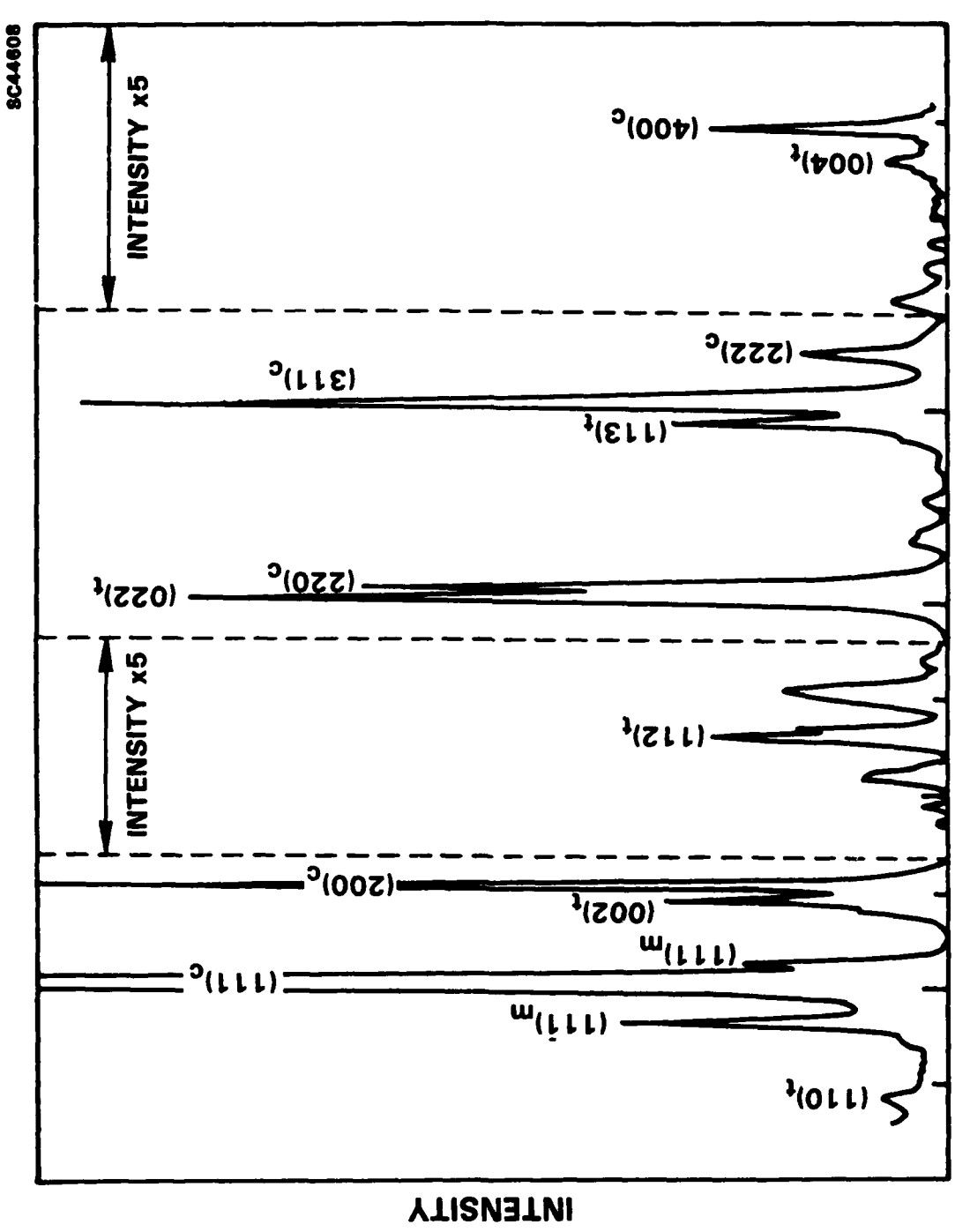
SC44608
INTENSITY x5
INTENSITY x5
(400)c
(004)t
(222)c
(311)c
(113)t
(220)c
(022)t
(112)t
(200)c
(002)t
(111)m
(111)c
(11$\bar{1}$)m
(110)t
INTENSITY
20
30
50
60
70
80
2θ (deg)

(A)

Figure 6(A)

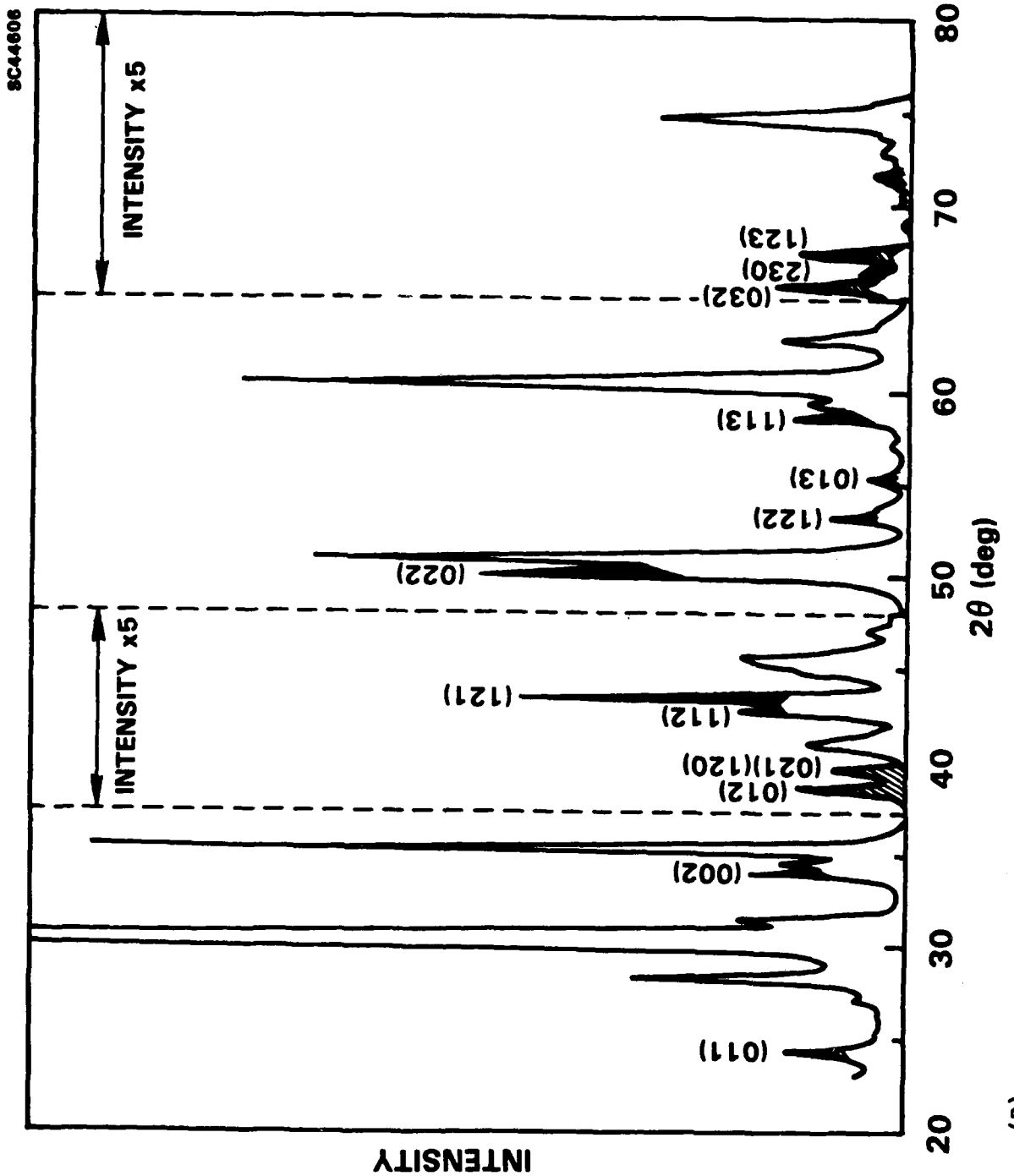
SC4460E
INTENSITY x5
INTENSITY x5
(123)
(230)
(032)
(113)
(013)
(122)
(022)
(121)
(112)
(021)(120)
(012)
(002)
(011)
INTENSITY
20
30
40
50
60
70
80
2θ (deg)
(B)

Figure 5(B)

SC44607
AS RECEIVED
AFTER COOLING IN LIQUID N_2
$(113)_c$
$(131)_t$
$(131)_o$
$(113)_t$
$(113)_o$
INTENSITY
58
59
60
61
2θ

(c)

Figure 6(c)

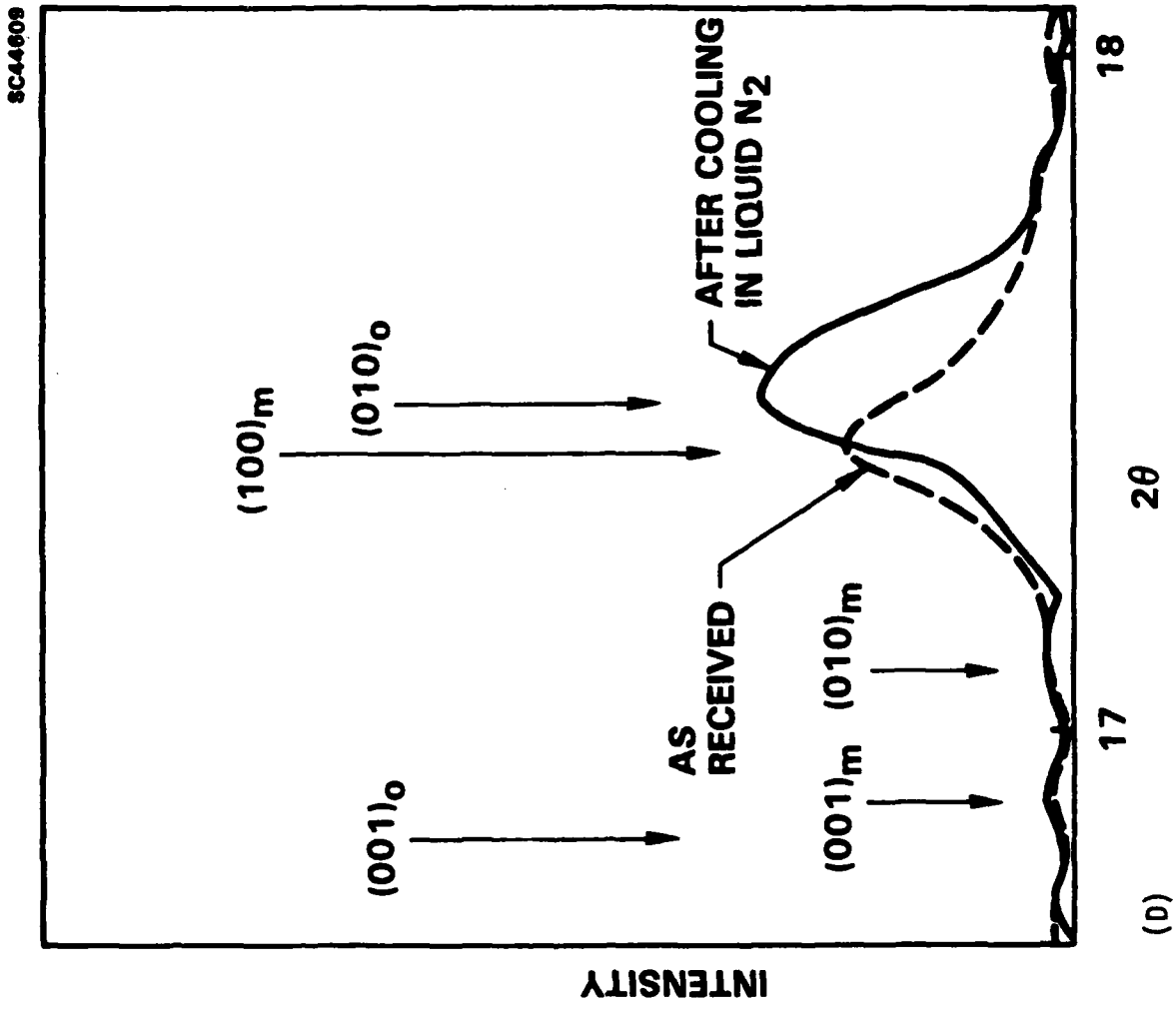
SC4460B
AFTER COOLING IN LIQUID N_2
$(100)_m$
$(010)_o$
AS RECEIVED
$(010)_m$
$(001)_m$
$(001)_o$
18
17
2θ
(D)
INTENSITY

Figure 6(D)

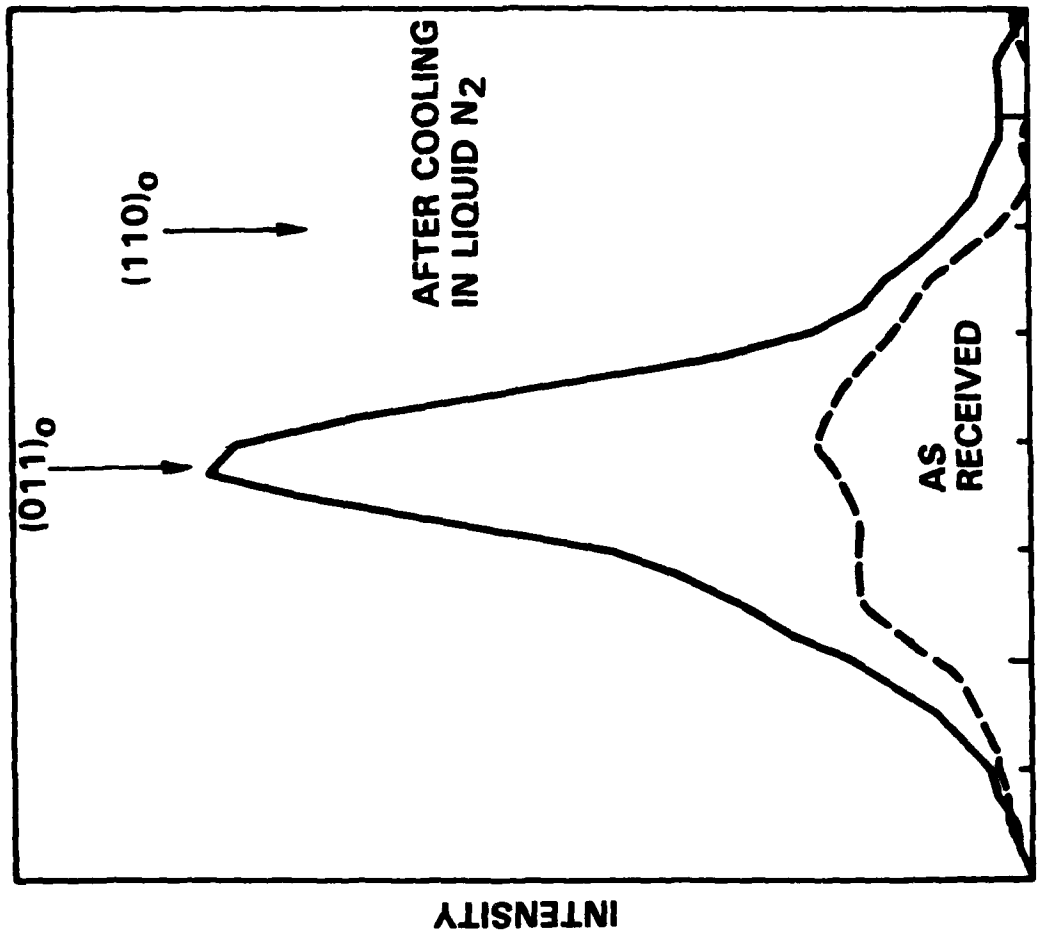
AFTER COOLING
IN LIQUID N_2
$(110)_o$
$(011)_o$
AS
RECEIVED
25
24
2θ
(E)
INTENSITY

Figure 6(E)

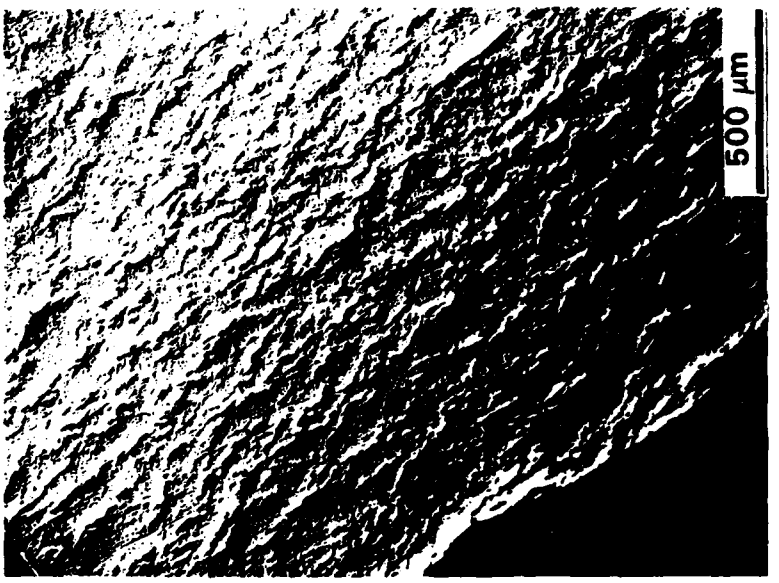
500 μm


500 μm

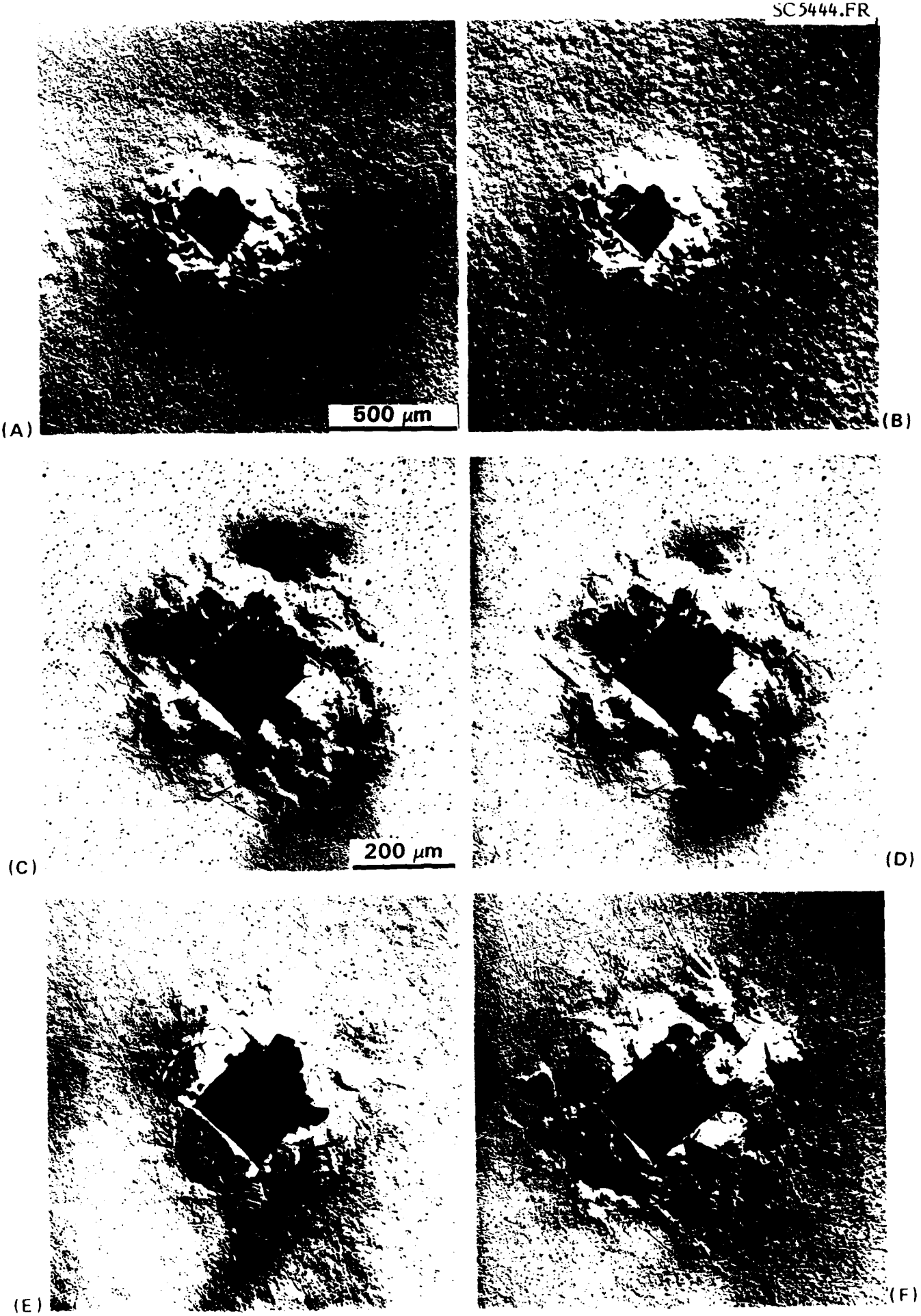

Figure 8A-F

C9734HA/ejw

Rockwell International
Science Center
SC5444.FR
SC42602
COUNTS x 10³
WAVENUMBERS (cm⁻¹)
120
145
176
186
222
262

Figure 9

SC42501

SC5444.FR

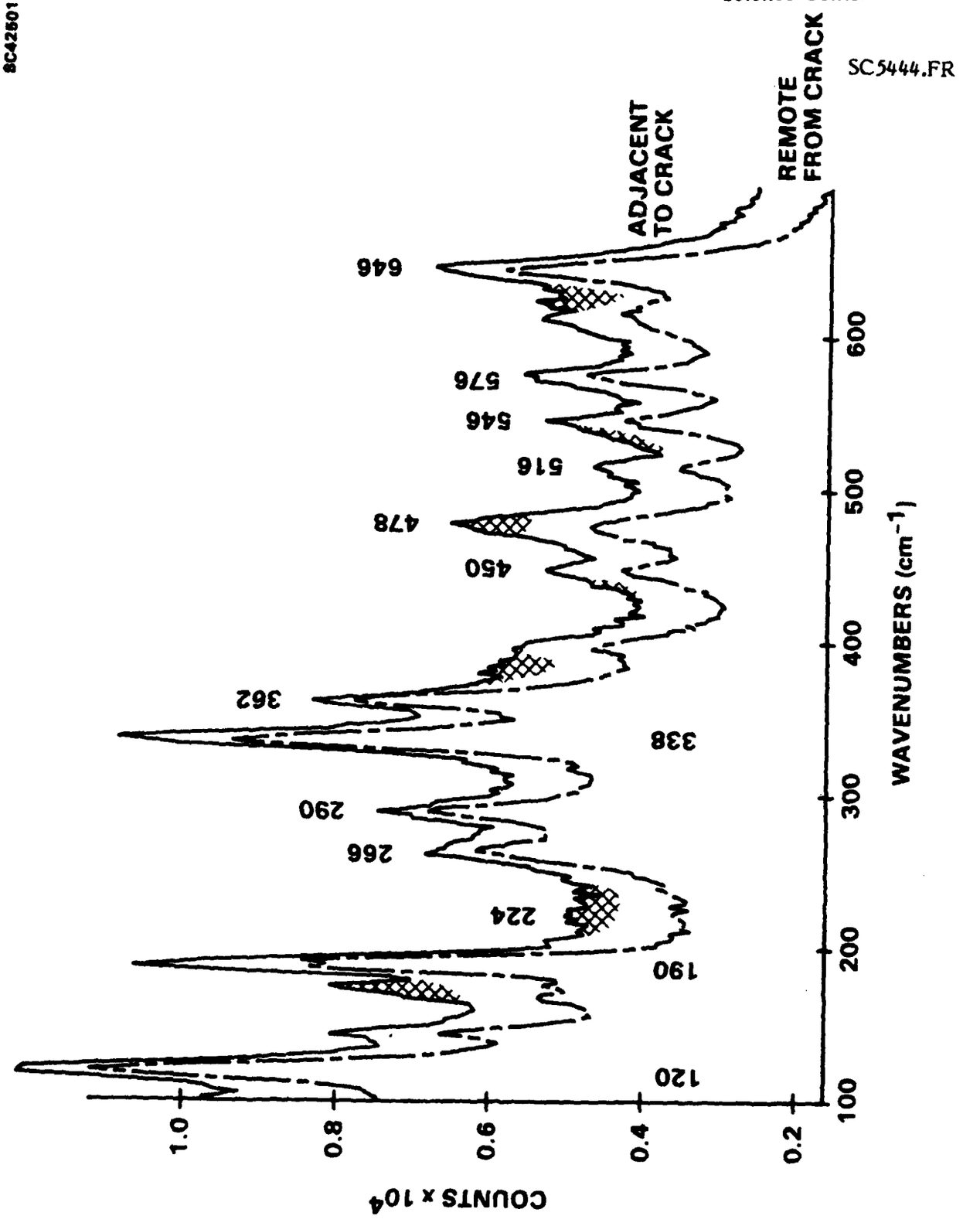

Figure 10

4.0 REVERSIBLE TRANSFORMATION AND ELASTIC ANISOTROPY IN Mg-PSZ*

*Submitted to the Journal of the American Ceramic Society.

Rockwell International
Science Center

SC5444.FR

REVERSIBLE TRANSFORMATION AND ELASTIC ANISOTROPY IN Mg-ZrO_2

D.B. Marshall
Rockwell International Science Center
1049 Camino Dos Rios
Thousand Oaks, CA 91360

and

M.V. Swain
Division of Materials Science
CSIRO
Clayton
Victoria 3168
Australia

ABSTRACT

Mechanical loading of polycrystalline ZrO_2 ceramics causes reversible, out-of-plane distortions at free surfaces that are parallel to the direction of applied stress. These distortions have been measured using optical interference microscopy, and the separate contributions due to elastic anisotropy and reversible martensitic transformation have been identified.

1.0 INTRODUCTION

Several studies have shown that the martensitic transformation in ZrO_2, between tetragonal and monoclinic phases, can occur reversibly with stress under certain conditions.[1-5] This observation is important for understanding the initiation condition for the transformation, which in turn determines the extent of the transformation zone around a crack and hence the degree of toughening.

The first indication of reversibility came from observations, by Nomarski interference, of surface distortions caused by varying amounts of transformation in adjacent grains. These measurements, from the polished surface of polycrystalline Mg-ZrO_2, were confirmed by in situ x-ray diffraction.[1] In situ TEM observations have also revealed reversible transformations in other ZrO_2 alloys.[2-5] Although the surface distortion measurement remains the most sensitive of these methods for detecting small amounts of transformation, it is complicated by the fact that distortion of the surface under applied load can also be caused by elastic anisotropy. In this paper measurements of the separate contributions to surface distortions in Mg-PSZ from elastic anisotropy and reversible transformation are presented.

2.0 EXPERIMENTAL OBSERVATIONS

Surface distortions were compared in one transformation toughened 9 mole% MgO-ZrO_2 material* and four related, nontoughened materials; (1) a fully stabilized cubic Mg-ZrO_2 (14 mole% MgO); (2) 3 mole% MgO-ZrO_2 which contained tetragonal

*MS grade Mg-PS2, Nitera, St. Charles, IL.

precipitates that were not sufficiently transformable to cause significant transformation toughening; (3) an overaged 9 mole% $MgO-ZrO_2$ in which all precipitates were of monoclinic phase; and (4) the toughened 9 mole% $MgO-ZrO_2$ which had undergone a cooling cycle in liquid nitrogen to transform most tetragonal precipitates to orthorhombic phase.[6] Of the nontoughened materials, the 9 mole% $MgO-ZrO_2$ cooled in liquid nitrogen possessed the highest strength (500 MPa, c.f. approximately 250 MPa for the others) and therefore allowed comparisons with the toughened material over the widest range of stresses. It was also closest to having an identical microstructure to that of the toughened material, but with the transformation switched off.

Beams of each material (~ 50 × 3 × 3 mm) were loaded in bending using fixtures on the stages of two optical microscopes, one fitted with Nomarski interference and the other with conventional interference using monochromatic light. While Nomarski interference is the more convenient and possibly the more sensitive of these two methods of observing surface distortions, it is qualitative. On the other hand, quantitative measurements of surface displacements are obtained from the conventional interference microscope. In the present experiments comparisons of the different materials were made using micrographs obtained with identical microscope settings and film/print processing. Applied stresses were monitored in all cases using strain gages attached to the surfaces of the beams.

The tensile surfaces of all five materials exhibited reversible distortions during loading. Observations in the fully stabilized, overaged, and 3.9 mole% MgO materials were limited (by their strengths) to applied stresses below approximately 200 MPa (i.e., strain < 0.001). Over this range of stresses the magnitudes of the surface distortions were indistinguishable in all of the materials. However, at larger applied stresses the magnitudes of the surface distortions were higher in the toughened material than in the

material that had been cooled in liquid N_2. Nomarski interference micrographs from these two materials are compared in Fig. 1 and measured surface displacements from conventional interference are shown in Fig. 2. (The relative surface displacements in Fig. 2 represent measurements of the largest height difference within sub areas approximately 200 × 200 μm on the tensile surfaces.) These results suggest that, at stresses below ~ 200 MPa, the surface distortions result from elastic anisotropy, but that at higher stresses in the toughened material, transformation strains and elastic anisotropy contribute about equally to the surface distortions.

In situ observation during continuous loading of the toughened material indicated that the same grains were either uplifted or depressed over the entire range of strains in Fig. 2, i.e., the magnitudes of the surface displacements increased monotonically with load everywhere. This indicates that the crystallographic orientations of distortions due to elastic anisotropy and transformation strains are similar.

3.0 DISCUSSION

3.1 Elastic Anisotropy

An applied stress parallel to the surface of a polycrystalline body causes contraction normal to the surface by an amount which, because of elastic anisotropy, is dependent upon the grain orientation. Therefore, the surface must become distorted where grains of different orientations meet. A detailed calculation of the magnitude of these distortions would be complex because all components of local stress and strain are nonuniform and dependent upon relative orientations of all adjacent grains. However, a rough estimate of the maximum distortion can be obtained by calculating the maximum and minimum Poisson's ratios and assuming uniform strain parallel to the applied stress.

For cubic ZrO_2 with elastic stiffness constants C_{11} = 417 GPa, C_{12} = 82 GPa, and C_{44} = 47 GPa,[7] the Young's moduli and maximum and minimum Poisson's ratios for applied stresses in the directions [100], [110], and [111] are listed in Table 1. Qualitatively, the elastic response of this material is similar to that of a structure composed of rods along the edges of a cube and hinged at the corners; it is stiffest when loaded along [100], soft when loaded along [111] and [110], and the transverse contraction (for tensile load) when loaded along [110] is large along $[1\bar{1}0]$ and very small along [001]. Therefore, the largest difference in contraction should be between grains with [110] parallel to the applied stress and $[1\bar{1}0]$ or [001] normal to the surface. For strain of 0.0015 parallel to [110], the difference in contraction (unconstrained) of the two grains would be $\Delta\epsilon$ = 0.0007. The grain size of this material is ~ 50 μm. Therefore, the difference in surface displacements would be ~ 350Å, consistent with the measurements in Fig. 2 for the material that had been cooled in liquid N_2.

3.2 Surface Distortions and Transformation Strains

In the spirit of the approximate calculations of the previous section, an upper bound can be estimated for the relative surface displacements due to transformation, assuming coupling between the transformation strain and the applied shear stress. Each grain in Mg-PSZ contains small, lens-shaped precipitates of tetragonal ZrO_2 in a solute-rich cubic matrix, with the tetragonal c-axis of the precipitates parallel to their smallest dimension. The precipitates are in three orientations, each with the tetragonal c-axis parallel to one of the cubic axes. If a single lattice correspondence for the martensitic t → m transformation is assumed (e.g., lattice correspondence C for which the tetragonal c-axis becomes the monoclinic c-axis),[8] then applied stress along a [110] direction provides the most favorable orientation for coupling with the shear strains. Then two sets

of precipitates are oriented with Schmidt factors of 0.5 for (001)/[100] transformation shear, and the third set have zero shear stress on the (001) plane. In this orientation, transformation of equal numbers of the two sets of favorably oriented precipitates uniformly throughout the grain causes total unconstrained strains of the grain

$$\varepsilon_x = f(e^T/3 + \gamma/2)$$

$$\varepsilon_y = f(e^T/3 - \gamma/2)$$

$$\varepsilon_z = f\, e^T/3 \qquad (1)$$

where x, y and z correspond to [110], $[1\bar{1}0]$ and [001], f is the volume fraction of transformed precipitates, and γ and e^T are the unconstrained shear and dilation strains of the transformation. The dilation strain is fixed at ~ 0.04, whereas the shear strain, which can be partly relieved by twinning, could take any value between zero and that of a single untwinned variant (0.15). Therefore, the largest depression of the surface occurs at grains with untwinned precipitates and oriented with [110] parallel to the applied stress and $[1\bar{1}0]$ normal to the surface. This is the same orientation as for the largest depression from elastic anisotropy, and is therefore consistent with the observations of the previous section. An upper bound for the magnitude of the surface distortion (unconstrained) due to transformation in these grains is given by the difference of ε_x amd ε_y in Eq. (1): with f = 0.03 at applied strain 0.0015, as measured previously using x-ray diffraction,[1] this gives $\Delta\varepsilon = 0.002$. Therefore, for a grain size of 50 μm the difference in surface displacement is ≈ 1000Å. This is adequate to account for the observed displacements due to transformation (Fig. 2).

4.0 CONCLUSIONS

Mechanical load applied parallel to the free surface of polycrystalline Mg-ZrO_2 ceramics causes reversible distortions of the surface. In nontoughened materials, and in transformation toughened material at low loads (≤ 200 MPa) the distortions are a result of elastic anisotropy and relative grain misorientations. At higher loads in the transformation toughened material, reversible martensitic transformation causes superimposed displacements with a similar magnitude and grain orientation dependence as the displacement due to elastic anisotropy. Therefore, although in situ observation of these distortions is a convenient method for detecting reversible transformation, care is needed to separate the influence of elastic anisotropy when interpreting the results. Furthermore, the observations of surface distortions due to elastic anisotropy serve to illustrate the nonuniformity of local stresses in polycrystalline bodies, even those with cubic structure, and the potential role of these local stresses in initiation of strength limiting cracks.

ACKNOWLEDGMENTS

Funding for this work was supplied by the Air Force Office of Scientific Research under Contract No. F49620-85-C-0143.

REFERENCES

1. D.B. Marshall and M.R. James, "Reversible Stress Induced Martensitic Transformation in ZrO_2," J. Am. Ceram Soc. 69(3) 215-217 (1986).

2. L. Ma, M.L. Mecartney and M. Rühle, to be published.

3. R.R. Lee and A.H. Heuer, "Thermoelastic Martensitic Transformation in (Mg, Y) PSZ," J. Am. Ceram. Soc., in press.

4. R.R. Lee and A.H. Heuer, "In Situ Martensitic Transformation in a Ternary MgO-Y_2O_3-ZrO_2 Alloy: I, Transformation in Tetragonal ZrO_2 Grains," J. Am. Ceram. Soc. 71(8), 694-700 (1988).

5. R.R. Lee and A.H. Heuer, "In Situ Martensitic Transformation in a Ternary MgO-Y_2O_3-ZrO_2 Alloy: II, Transformation in Tetragonal ZrO_2 Precipitates," J. Am. Ceram. Soc. 71(8), 701-706 (1988).

6. D.B. Marshall, M.R. James and J.R. Porter, "Structural and Mechanical Property Changes in Toughened Mg-PSZ at Low Temperatures," J. Am. Ceram. Soc., in press.

7. A.H. Heuer and M. Rühle, "On the Nucleation at the Martensitic Transformation in Zirconia (ZrO_2)," Acta. Metall. 33(12), 2101-12 (1985).

8. R.P. Ingel and D. Lewis III, "Elastic Anisotropy in ZrO_2 and Other Single Crystal Oxides," J. Am. Ceram. Soc., in press.

9. W.M. Kriven, W.L. Fraser and S.W. Kennedy, "The Martensitic Crystallography of Tetragonal Zirconia," Science and Technology of Zirconia, Advances in Ceramics 3, 82-97, The American Ceramic Society, Columbus, OH (1981).

Table 1

Young's Modulus and Poisson's Ratio of Cubic ZrO_2

Stress Direction	E	ν	
	(GPa)	Max	Min
[100]	390	0.16	
[110]	156	0.66 $(1\bar{1}0)$	0.08(001)
[111]	130		

Figure Captions

1. Optical micrographs (Nomarski interference), comparing out-of-plane surface distortions in (a) transformation toughened Mg-PSZ and (b) nontoughened Mg-PSZ. Applied load horizontal, average strain 0.0015.

2. Relative surface displacements, measured by optical interference microscopy for toughened (as-received) and nontoughened (cooled in liquid N_2) Mg-PSZ.

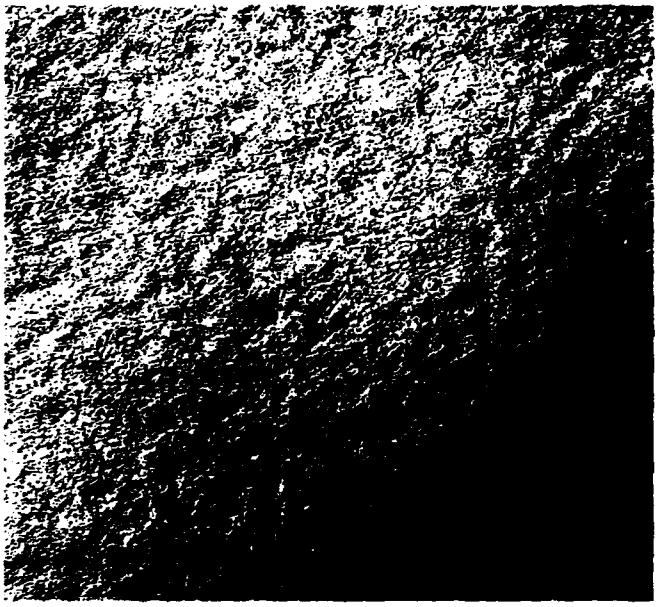

(B)

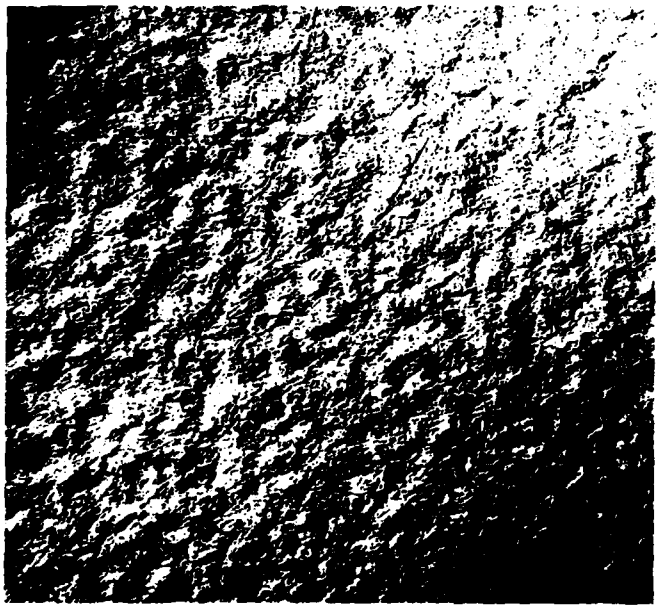

(A)

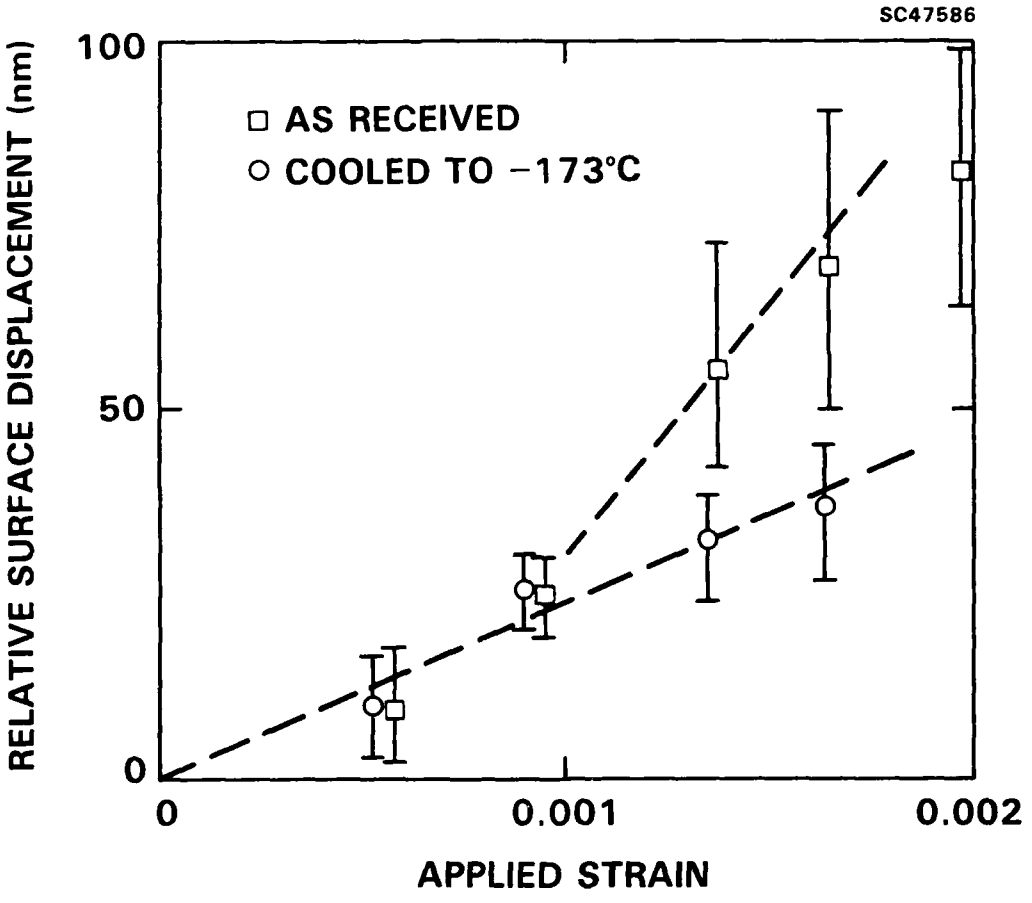
SC47586
RELATIVE SURFACE DISPLACEMENT (nm)
100
50
0
□ AS RECEIVED
○ COOLED TO −173°C
0
0.001
0.002
APPLIED STRAIN

5.0 CYCLIC FATIGUE CRACK PROPAGATION IN CERAMICS: BEHAVIOR IN OVERAGED AND PARTIALLY STABILIZED MgO-ZrO_2*

*To be published in MRS Proceedings, Symposium on Fracture Mechanics of Ceramics.

CYCLIC FATIGUE-CRACK PROPAGATION IN CERAMICS: BEHAVIOR IN OVERAGED AND PARTIALLY-STABILIZED MgO-ZIRCONIA

SC5444.FR

R. H. DAUSKARDT*, D. B. MARSHALL** and R. O. RITCHIE*
*Center for Advanced Materials, Lawrence Berkeley Laboratory, and Department of Materials Science and Mineral Engineering, University of California, Berkeley, CA 94720
**Rockwell International Science Center, Thousand Oaks, CA 91360

ABSTRACT

The growth of fatigue cracks under (tension-tension) cyclic loading is unequivocally demonstrated for ceramic materials, based on experiments using compact-tension specimens of a MgO partially-stabilized zirconia (PSZ), heat treated to vary the fracture toughness K_c from $\sim$3 MPa$\sqrt{m}$ (overaged condition) to 16 MPa$\sqrt{m}$ (peak-toughness condition) and tested in inert and moist environments. Analogous to behavior in metals, cyclic fatigue-crack growth rates (over the range 10^{-11} to 10^{-5} m/cycle) are found to be a function of the stress-intensity range, environment, fracture toughness and load ratio, and to show evidence of crack closure. Similarly under variable-amplitude cyclic loading conditions, crack-growth rates show transient accelerations following low-high block overloads and transient retardations following high-low block overloads or single tensile overloads, again analogous to behavior commonly observed in ductile metals. Cyclic crack-growth rates are observed at stress intensities as low as 50% of K_c, and are typically some 7 orders of magnitude faster than corresponding stress-corrosion crack-growth rates under sustained-loading conditions.

INTRODUCTION

The projected use of ceramics rather than metallic materials for structural applications, such as in gas-turbine engines, has been motivated by their low density, far superior elevated-temperature strength and presumed insensitivity to degradation from cyclic fatigue [1]. However, several investigations [2-7] utilizing smooth specimens, sometimes containing indentation flaws, tested under rotating bending, four-point bending or by repeated thermal stressing, have shown reduced lifetimes for alumina, zirconia-alumina, TZP and silicon nitride under cyclic, as opposed to static, loading conditions. Moreover, subcritical crack growth has been reported for several monolithic and composite ceramics tested under far-field cyclic compression loads [8,9]. Although several explanations have been suggested for such apparent fatigue behavior, including deformation and lateral cracking of crack-surface asperities on unloading [1,6], tensile opening from the wedging action of such asperities [1] or corrosion debris [10], friction-induced heating at the crack tip [11], and environmentally-assisted (stress-corrosion) cracking processes [6,10,11], there are few examples of unequivocal demonstrations of a true cyclic fatigue phenomenon in ceramics [1].

The refuted existence of a true fatigue effect in ceramics has been based primarily on their very limited crack-tip plasticity. Recently however, based on the premise that other inelastic deformation mechanisms may prevail in these materials, such as microcracking, transformation "plasticity" or frictional sliding between a reinforcement phase and the ceramic matrix, Dauskardt et al. [11] provided the first persuasive evidence of true cyclic fatigue-crack growth in a MgO partially-stabilized zirconia (MgO-PSZ) ceramic, which had been marginally transformation toughened to a K_c of 5.5 MPa$\sqrt{m}$. Their results, which have been subsequently confirmed by Swain et al. [7] in a commercial MS-Grade MgO-PSZ, indicated that crack-growth

rates were a power-law function of the stress-intensity range ΔK, with an exponent m of ~ 24, were sensitive to frequency and load ratio ($R = K_{min}/K_{max}$), and showed evidence of crack closure [12], analogous to behavior in metals.

In the present study, a more extensive examination of cyclic fatigue-crack growth in MgO-PSZ is undertaken to investigate: i) how fatigue resistance varies with microstructures of differing fracture toughness, ii) the role of environment on crack-growth rates, and iii) the nature of transient fatigue behavior following specific variable-amplitude cyclic loading sequences (i.e., post-overload behavior).

EXPERIMENTAL PROCEDURES

Tests were performed on precipitated partially-stabilized zirconia, containing 9 mol% magnesia (MgO-PSZ), chosen for its transformation-toughening behavior [13-16]. The microstructure consists of cubic ZrO_2 grains, ~ 50 μm in diameter, with lens-shaped tetragonal precipitates of maximum size 300 nm; up to 40% of the latter phase can undergo a stress-induced martensitic transformation due to the high stresses near the crack tip [16]. The MgO-PSZ was examined in four microstructural conditions, selected to vary the fracture toughness from a K_C of 2.9 MPa$\sqrt{m}$ in the overaged (non-transformation-toughened) condition to 16 MPa$\sqrt{m}$ in the peak-toughened condition. The heat treatments, together with respective ambient-temperature mechanical properties, are listed in Table I. Further details of the microstructural and mechanical-property characteristics of this material are described elsewhere [13-16].

Table I. Heat Treatments and Tensile Properties of MgO-PSZ

Condition	Heat Treatment	Young's Modulus, E (GPa)	Approx. Tensile Strength (MPa)	Fracture Toughness K_i (MPa$\sqrt{m}$)*	Fracture Toughness K_C (MPa$\sqrt{m}$)*
overaged	24 h at 1100°C	<200	300	2.5	2.9
low toughness	as received	208	300	~ 3	5.5
mid toughness	3 h at 1100°C	208	600	~ 3	11.5
peak toughness	7 h at 1100°C	208	400	~ 4	16.0

*K_i and K_C are the initiation and plateau toughness values from the R-curve.

Fatigue-crack propagation studies were performed on 3-mm-thick compact tension C(T) specimens, containing long (> 3 mm) through-thickness cracks, which were cyclically loaded at a load ratio of 0.1 and frequency of 50 Hz (sine wave) in high-resolution, computer-controlled electro-servohydraulic testing machines. Crack initiation was facilitated by a wedge shaped starter notch. Testing was performed in controlled room air (22°C, 45% relative humidity), dehumidified gaseous nitrogen and distilled water environments. Electrical-potential measurements across ~ 0.1-μm NiCr foils, evaporated onto the specimen surface, were used *in situ* to monitor crack lengths to a resolution better than 5 μm; unloading compliance measurements using back-face strain gauges were similarly used to assess the extent of fatigue crack closure in terms of the stress intensity K_{cl} at first contact of the fracture surfaces during the unloading cycle [17]. Crack-growth rates, da/dN, were determined over the range 10^{-11} to 10^{-5} m/cycle under both manual and computed-controlled K-decreasing and K-increasing conditions, with a

normalized K-gradient of 0.80 mm^{-1} [18]; data are presented in terms of the applied stress-intensity range ($\Delta K = K_{max} - K_{min}$, where K_{max} and K_{min} are, respectively, the maximum and minimum stress intensities in the fatigue cycle). Fracture toughness values were measured from $K_R(\Delta a)$ resistance curves, determined by monotonically loading the fatigue-cracked C(T) specimens. Further experimental details are given elsewhere [11].

RESULTS AND DISCUSSION

Role of Fracture Toughness: Resistance curves for the four microstructures are illustrated in Fig. 1a. Whereas the overaged microstructure is fully transformed by heat treatment and shows only a shallow R-curve with a K_C of 2.9 MPa$\sqrt{m}$, the other PSZ microstructures undergo transformation toughening resulting in (plateau) toughnesses of 5.5 to 16 MPa$\sqrt{m}$. Note that as the R-curves were obtained in each specimen after the fatigue test, the full R-curves are not observed but begin at the final K_{max} of the ΔK range employed in the previous fatigue cycling. Corresponding cyclic fatigue-crack propagation data are plotted in Fig. 1b as a function of the stress-intensity range ΔK for a controlled room-air environment. It is apparent that growth rates show a conventional Paris law relationship [19]:

$$da/dN = C\,(\Delta K)^m , \qquad (1)$$

where the exponent m is in the range 21 to 42, and the constant C scales with the fracture toughness. Surprisingly, the overaged material in which the nonlinear deformation behavior associated with transformation plasticity has been removed, displays extensive cyclic fatigue-crack propagation behavior, with a similar power-law dependency on the stress-intensity range exhibited by the toughened materials. Moreover, the present data indicate that the overaged microstructure exhibits fatigue-crack growth at stress intensities below that required for crack initiation under monotonic loading on the R-curve. In fact, each set of data shows an apparent threshold, ΔK_{TH}, below which crack growth is presumed dormant; the value of ΔK_{TH} is seen to be approximately $\frac{1}{4}K_C$. Values of C, m and ΔK_{TH} for each microstructure are listed in Table II. It is apparent that resistance to cyclic fatigue-crack growth in MgO-PSZ is enhanced with increasing fracture toughness.

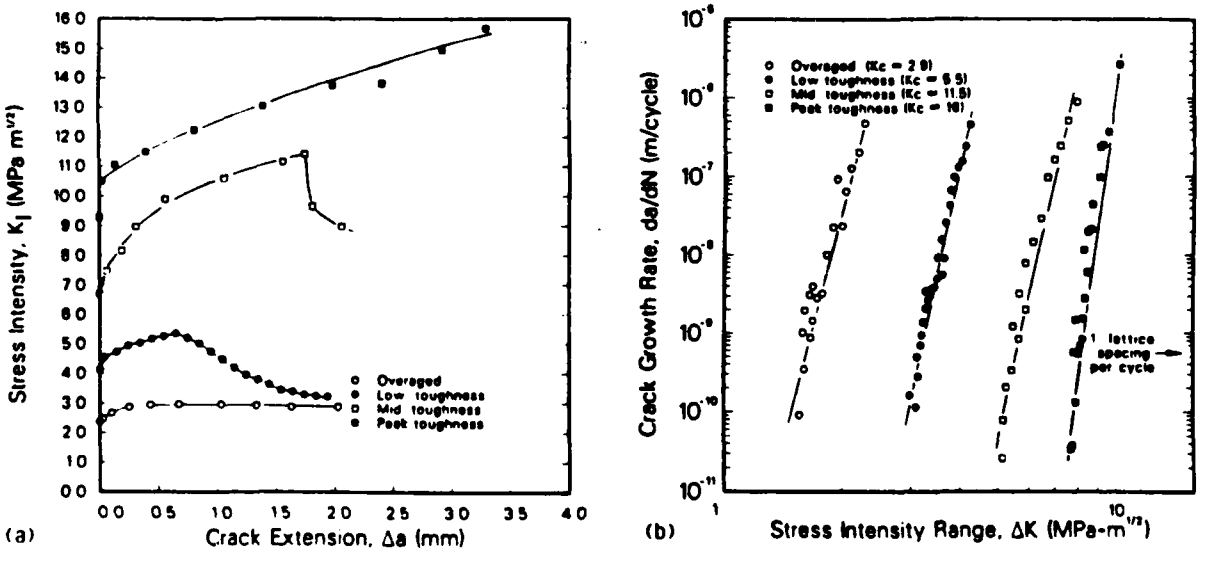

Fig. 1: Fracture-toughness and cyclic fatigue-crack growth behavior of MgO-PSZ heat treated to a range of toughnesses, showing a) $K_R(\Delta a)$ resistance curves, and b) crack-growth rates da/dN as a function of the stress-intensity range ΔK (room air environment at R = 0.1).

Table II. Values of C and m (in Eq. 1) and the Threshold ΔK_{TH} in MgO-PSZ

Condition	K_C (MPa$\sqrt{m}$)	C (MPa$\sqrt{m}$.m/cycle)	m	ΔK_{TH} (MPa$\sqrt{m}$)*
overaged	2.9	2.00×10^{-14}	21	1.6
low toughness	5.5	4.89×10^{-22}	24	3.0
mid toughness	11.5	5.70×10^{-28}	24	5.2
peak toughness	16.0	1.70×10^{-48}	42	7.7

*ΔK_{TH} defined at a maximum growth rate less than 10^{-10} m/cycle [18].

As described elsewhere [11], such fatigue-crack growth behavior in PSZ is *cyclically* induced and not simply subcritical cracking at maximum load. Tests on the low-toughness microstructure at constant K_{max}, where growth-rate behavior was monitored i) when the load was cycled between K_{max} and K_{min} (R = 0.1) compared to being held constant at K_{max} (Fig. 2), and ii) when the value of K_{min} was varied, clearly indicated a true cyclic fatigue phenomenon with growth rates proportional to the *range* of stress intensity. In fact as shown below (Fig. 5a), under constant ΔK conditions, fatigue-crack growth rates in MgO-PSZ remain essentially constant.

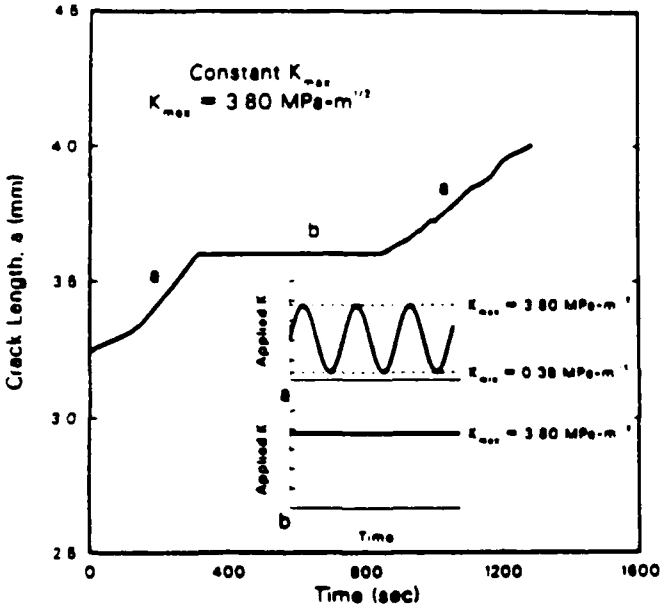

Fig. 2: Effect in low-toughness MgO-PSZ of sustained and cyclic loading conditions on subcritical crack-growth rates at a constant K_{max} of 3.8 MPa$\sqrt{m}$ [11].

Role of Environment: It has been suggested that fatigue in ceramics may alternatively be the result of stress-corrosion cracking [6,10,11]. To examine this hypothesis, cyclic crack-growth rates in the low-toughness microstructure were additionally measured in inert (dehumidified nitrogen gas) and corrosive (distilled water) environments; results are plotted as a function of ΔK in Fig. 3. As expected, growth rates are progressively faster in moist room air and water compared to inert nitrogen gas, indicating a marked corrosion-fatigue effect presumably involving the weakening of atomic bonds at the crack tip by adsorbing water molecules; however, crack growth is still observed in the inert atmosphere implying that, analogous to behavior in metals, *cyclic fatigue in the ceramic is a mechanically-induced cyclic process which may be accelerated by the environment.*

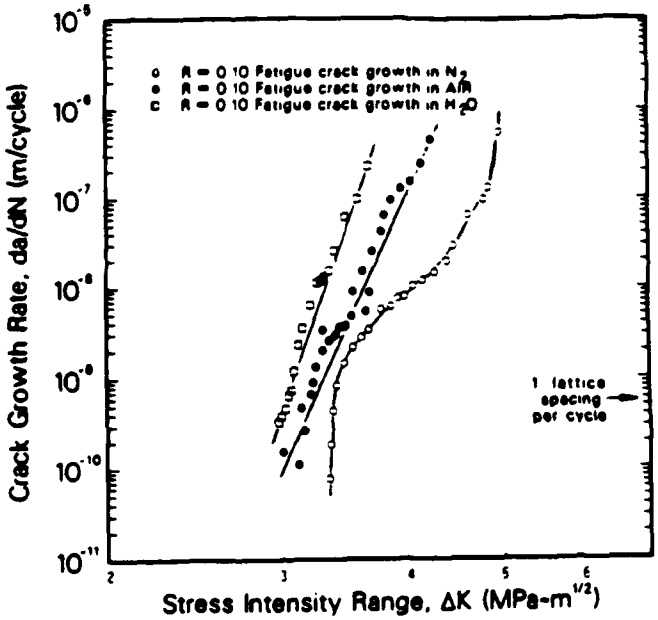

Fig. 3. Cyclic fatigue-crack growth rates da/dN as a function of ΔK in low-toughness MgO-PSZ in dry nitrogen gas, room air and distilled water, showing an acceleration in growth rates due to water vapor.

Mechanisms: Crack-Tip Shielding: As described in ref. 11, fatigue-crack growth in PSZ fractographically resembles monotonic overload failures with a predominantly transgranular fracture morphology and no evidence of fatigue striations. Crack-path morphologies, however, do show evidence of crack-tip shielding from frequent crack deflection and crack bridging from uncracked ligaments just behind the crack tip. In addition, analogous to behavior in metals, back-face strain compliance measurements gave clear indications of fatigue crack closure, with K_{cl}/K_{max} ratios varying from almost 0.4 close to ΔK_{TH} to ~0.1 close to K_c [11]. In view of the deflected nature of the crack paths, it is presumed that such closure results primarily from the wedging action of fracture-surface asperities (roughness-induced crack closure [12,20]). Evidence for shielding by transformation toughening, conversely, can be seen by examining the inelastic transformed zones that surround the crack using spatially-resolved Raman spectroscopy or Normaski techniques [21]; a three-dimensional Raman plot of such a zone in peak-toughness MgO-PSZ, both ahead and in the wake of the crack tip, is shown in Fig. 4. However, to date we have been unable to detect whether such zones are different in size or morphology for cyclically, as opposed to monotonically, loaded cracks at the same stress-intensity level.

Role of Variable-Amplitude Loading: The results described above pertain solely to constant-amplitude cyclic loading; to examine the influence of variable-amplitude loading, single and block overload sequences were applied during steady-state fatigue-crack growth in the mid- and peak-toughness MgO-PSZ materials. Results for high-low and low-high block overloads in mid-toughness material are shown in Fig. 5a. Over the first ~2.5 mm of crack advance, the crack-growth rate remains approximately constant under constant ΔK (= 5.48 MPa$\sqrt{m}$) conditions. On reducing the cyclic loads to a ΔK corresponding to 5.30 MPa$\sqrt{m}$ (high-low block overload), however, a marked transient retardation is seen followed by a gradual increase in growth rates until the (new) steady-state velocity is achieved. Similarly, by subsequently increasing the cyclic loads to a ΔK corresponding to 5.60 MPa$\sqrt{m}$ (low-high block overload), growth rates show an immediate transient acceleration before a decay to the steady-state velocity. Such behavior is exactly analogous to that widely observed in metals [22], where to the first order the crack-growth increment affected by the overload is comparable with the extent of the overload plastic zone. In the present experiments, the affected crack-growth increments are approximately 1 to 1.2 mm, slighly larger than five times the measured [21] transformed-zone width of 150 μm.

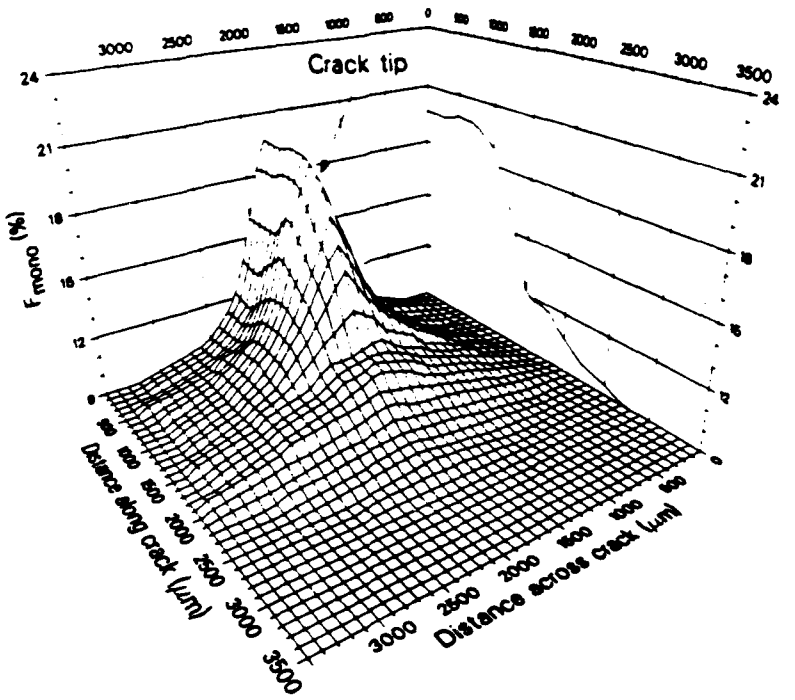

Fig. 4: Three-dimensional Raman spectroscopy plot of the morphology of the transformed zone both ahead, and in the wake of, the crack tip in peak-toughened MgO-PSZ. Plotted along the ordinate is the relative proportional of transformed (monoclinic) phase [21].

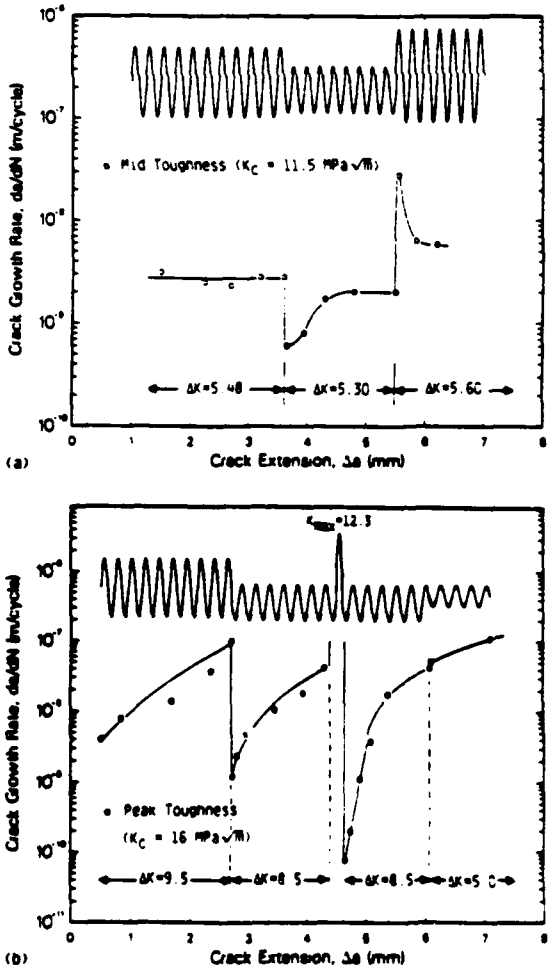

Fig. 5: Transient fatigue-crack growth behavior in a) mid-toughness and b) peak-toughness MgO-PSZ due to variable-amplitude cyclic loads, showing immediate crack-growth retardations following high-low block overloads, immediate accelerations following low-high block overloads, and delayed retardation following a single tensile overload (room air environment).

Similar crack-growth retardation following a high-low block overload (ΔK = 9.5 to 8.5 MPa$\sqrt{m}$) is shown for peak-toughness MgO-PSZ in Fig. 5b; in addition, significant *delayed* retardation can be seen following a single tensile overload to a K_{max} of 12.3 MPa$\sqrt{m}$. Such results can be rationalized in terms of measured changes in crack closure [23], and are again analogous to behavior in metals [22]. Further details are described in ref. 23.

Comparison with Stress-Corrosion Cracking Data: It is clear from the present results that cyclic fatigue-crack growth in ceramics can occur at stress intensities at low as $\frac{1}{4}K_C$. Moreover, compared to behavior under monotonic loading, cyclic crack-growth rates in MgO-PSZ can be many orders of magnitude faster, and can occur at stress intensities far lower, than that required for stress-corrosion cracking [11]. This is illustrated in Fig. 6 for the mid-toughness microstructure tested in moist air, where cyclic crack velocities, plotted as a function of time (da/dt), are compared with corresponding stress-corrosion crack velocities measured under sustained loads; at equivalent K levels cyclic crack-growth rates can be seen to be up to 7 orders of magnitude faster.

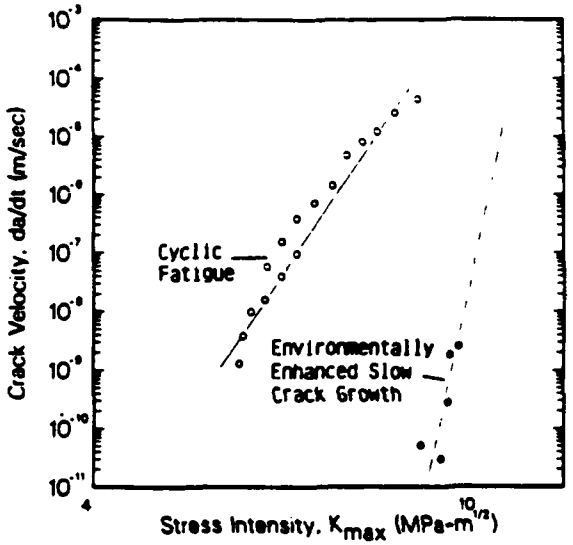

Fig. 6: Subcritical crack-growth behavior in mid-toughness MgO-PSZ, showing a comparison of crack velocities da/dt, as a function of K_{max}, measured under monotonic and cyclic loading conditions in a moist air environment. Note how the cyclic crack velocities are up to 7 orders of magnitude faster at equivalent stress-intensity levels.

It would thus appear that nonconservative estimates of the subcritical advance of incipient cracks, and serious overestimates of life, may result in PSZ ceramics if defect-tolerant predictions are based solely on sustained-load (stress-corrosion) and fracture-toughness data and do not consider a cyclic fatigue effect.

CONCLUSIONS

Based on a study of the growth of fatigue cracks in MgO-PSZ ceramics under tension-tension cyclic loads, the following conclusions can be made:

1. Fatigue-crack growth in overaged (microcrack toughened) and partially-stabilized (transformation toughened) zirconia is unequivocally demonstrated to be a mechanically-induced cyclic process, which is accelerated in moist air and distilled water environments. Growth rates (da/dN) are found to be primarily a power-law function of the stress-intensity range (ΔK), with an exponent m in the range of 21 to 42.

2. Superior cyclic crack-growth resistance is found when the fracture toughness (K_C) of MgO-PSZ is increased; the apparent threshold for fatigue-crack growth (ΔK_{TH}), below which cracks are dormant, is approximately $\frac{1}{4}K_C$.

3. Cyclic crack growth in ceramics shows evidence of crack closure. Moreover, when subjected to variable-amplitude cyclic loading, fatigue cracks in MgO-PSZ experience a transient crack-growth retardation immediately following high-low block overloads, a transient acceleration immediately following low-high block overloads, and a delayed retardation following single tensile overloads; such behavior is exactly analogous to that commonly reported for metallic materials.

4. Cyclic crack velocities in MgO-PSZ are found to be up to 7 orders of magnitude faster, and threshold stress intensities almost 50% lower, than stress-corrosion crack velocities measured in identical environments under sustained-loading conditions. Such observations may have serious implications for defect-tolerant life predictions in zirconia ceramics.

Acknowledgments

This work was supported by the Director, Office of Energy Research, Office of Basic Energy Sciences, Materials Sciences Division of the U.S. Department of Energy under Contract No. DE-AC03-76SF00098 and the Air Force Office of Scientific Research under Contract No. F49620-85-C-0143. The authors thank Drs. R.M. Cannon, R.J. Gottschall and W. Yu for helpful discussions, and Drs. D.K. Veirs and G.M. Rosenblatt for help with the Raman studies.

References

1. A. G. Evans, Int. J. Fract. 16, 485 (1980).
2. D. Lewis, Ceramic Engineering & Science Proc. 4, 874 (1983).
3. R. W. Rice, Amer. Ceram. Soc. Bull. 63, 256 (1984).
4. T. Kawakubo and K. Komeya, J. Am. Ceram. Soc. 70, 400 (1987).
5. M. V. Swain and V. Zelizko, in Advances in Ceramics (Amer. Ceram. Soc. 24, 1988) in press.
6. T. Kawakubo (Mat. Res. Soc. Symp. Proc., 1988) this volume.
7. M. V. Swain, V. Zelizko, S. Lam, and M. Marmach (Mat. Res. Soc. Symp. Proc., 1988) in press.
8. L. Ewart and S. Suresh, J. Mater. Sci. Lett. 5, 774 (1986).
9. S. Suresh, L. X. Han, and J. P. Petrovic, J. Am. Ceram. Soc. 71, C-158 (1988).
10. L. S. Williams, in Mechanical Properties of Engineering Ceramics, edited by W. W. Kriegel and H. Palmour (Interscience Publishers, New York, NY, 1961), Chapt. 18.
11. R. H. Dauskardt, W. Yu, and R. O. Ritchie, J. Am. Ceram. Soc. 70, C-248 (1987).
12. R. O. Ritchie, Mater. Sci. Eng. 103, (1988).
13. A. G. Evans and R. M. Cannon, Acta Metall. 34, 761 (1986).
14. R. H. J. Hannick and M. V. Swain, J. Aust. Ceram. Soc. 18, 53 (1982).
15. D. B. Marshall, J. Am. Ceram. Soc. 69, 173 (1986).
16. D. B. Marshall and M. R. James, J. Am. Ceram. Soc. 69, 215 (1986).
17. R. O. Ritchie and W. Yu, in Small Fatigue Cracks, edited by R. O. Ritchie and J. Lankford (TMS-AIME, Warrendale, PA, 1986), p. 167.
18. ASTM Standard E 647-86A, in ASTM Annual Book of Standards (American Soc. Test. & Matls. 3.01, Philadelphia, PA, 1987), p. 899.
19. P. C. Paris and F. Erdogan, J. Bas. Eng., Trans. ASME 85, 528 (1963).
20. S. Suresh and R. O. Ritchie, Metall. Trans. A 13A, 1627 (1982).
21. R. H. Dauskardt, D. K. Veirs, and R. O. Ritchie, J. Am. Ceram. Soc. 71, (1988) in review.
22. R. W. Hertzberg, Deformation and Fracture Mechancis of Engineering Materials, 2nd. ed. (Wiley, New York, NY, 1983).
23. R. H. Dauskardt, D. B. Marshall, and R. O. Ritchie, J. Mater. Sci. 23, (1988) in review.

6.0 CRACK TIP TRANSFORMATION ZONES IN TOUGHENED ZIRCONIA*

*To be submitted to the Journal of the American Ceramic Society.

SC5444.FR

CRACK TIP TRANSFORMATION ZONES IN TOUGHENED ZIRCONIA

D.B. Marshall and M.C. Shaw

Rockwell International Science Center
1049 Camino Dos Rios
Thousand Oaks, CA 91360

R. Dauskardt and R.O. Ritchie
Center for Advanced Materials
Lawrence Berkeley Laboratory
Berkeley, CA 94720

M. Readey and A.H. Heuer
Department of Metallurgy and Materials Science
Case Western Reserve University
Cleveland, OH 44106

ABSTRACT

Transformation zones surrounding cracks in several toughened Mg-PSZ ceramics are characterized by optical interference measurements of surface uplift and by Raman microprobe spectroscopy. The measurements demonstrate that the volume fraction of transformation is nonuniform within the zone and that the frontal zone is approximately defined by a contour of constant hydrostatic stress in the crack tip field. Results are used to evaluate the crack tip shielding stress intensity factor and to compare with measured fracture toughness.

1. INTRODUCTION

The fracture toughness of zirconia based materials can be increased by an order of magnitude (from ~ 2 MPa $m^{1/2}$ to 20 MPa $m^{1/2}$) by manipulating their microstructures to change the stability of retained tetragonal phases.[1-6] It is reasonably well established that at least a substantial portion of this toughening results from shielding of crack tips from the applied load by the strains resulting from a martensitic transformation from tetragonal-to-monoclinic phase within limited zones surrounding the cracks.[7] Such zones have been detected by several techniques: x-ray diffraction,[8] transmission electron microscopy (TEM),[9,10] Raman spectroscopy,[11,12] and observations by optical interference methods of surface distortions due to the transformation strains.[13-15] However, none of these methods have yet been used to provide quantitative measurements of transformation zone parameters (i.e., distributions of transformation, net transformation strain) that are needed for calculation of the toughening due to shielding.

Rigorous fracture mechanics analyses have been derived to relate the toughness increase due to shielding to the zone parameters. For a steady state crack (i.e., crack growth at constant applied stress intensity factor, K_a), with a zone containing a uniform volume fraction of transformation over a distance w from the crack surface, the shielding stress intensity factor is[7,16-18]

$$\Delta K_s = A\, f E e^T \sqrt{w} \qquad (1)$$

where E is the elastic modulus and e^T is the transformation strain. The constant A is equal to 0.3 if e^T is isotropic dilational strain and the frontal zone is defined by a contour of constant hydrostatic tension in the elastic crack tip field; deviation from

either of these assumptions modify this constant. If the amount of transformation is not uniform, ΔK_s can be evaluated by integration of Eq. (1):[19,20]

$$\Delta K_s = A\ E\ e^T \int_0^{w_o} \frac{f(x)}{2\sqrt{x}}\ dx \qquad (2)$$

where f(x) is the function representing the variation of the volume fraction of transformation with distance x from the crack and w_o is the distance from the crack at which no transformation occurs. It is important to note that these results are restricted to steady state cracks, with wake zones of constant width. In general, initial growth of a crack in these materials is dictated by an R-curve, with increasing zone width as the crack grows. It is also noteworthy that, while the fracture mechanics analyses are available to relate toughness to zone parameters, prediction of the zone parameters such as f(x), the frontal shape, and the net transformation strain is not presently possible.

Attempts to correlate toughness measurements with predictions of the mechanics analyses have been at best order-of-magnitude estimates because of inadequate measurement of zone parameters: most have calculated f and w assuming a step function for f(x) with complete transformation within the zone, using x-ray measurements from fracture surfaces of broken test pieces to estimate the zone size.[7,8,20] We will show that f(x) is not well approximated by a step function. Moreover, unless the fracture surface results from crack growth at constant applied stress intensity factor, zone width measurements from a large area of the fracture surface (as is the case for x-rays) are misleading. In this paper we present measurements of detailed distributions of transformation within zones around cracks that were grown under controlled and known stress intensity factors, and preliminary correlation of the amount of shielding with fracture mechanics predictions.

2. EXPERIMENTS

Precipitated partially stabilized zirconia containing 9 mole% MgO (i.e., Mg-PSZ) was chosen as the test material because the fracture toughness (and amount of shielding) can be varied over a wide range by subeutectoid heat treatment. Fabrication, heat treatment, and microstructures have been described by Hannink[5] and Hannink and Swain:[6] the microstructures are composed of cubic ZrO_2 grains ~ 50 μm in diameter containing lens-shaped tetragonal precipitates (~ 40 vol.%) with largest dimension ~ 300 nm. The subeutectoid heat treatment does not significantly alter the microstructural dimensions, but it is known to cause a decomposition reaction resulting in growth of a magnesia-rich δ phase at the precipitate boundaries which is thought to destabilize the tetragonal phase.

Transformation zones surrounding cracks grown under known loading conditions in compact tension fracture mechanics specimens were characterized by two methods: interference microscopy and Raman spectroscopy. The optical interference measurements were obtained from the faces of the compact tension specimens which had been polished prior to introduction of the cracks. The surface displacements provide a measure of the transformation strains. The Raman spectroscopy from the same surface provides a direct measurement of the fractions of tetragonal and monoclinic phases.

Two optical interference methods were used: Nomarski interference and conventional interference. Nomarski interference provides a qualitative indication of changes in the inclination of the surface, whereas the conventional interference provides a direct quantitative measure of the normal surface displacement.

Raman measurements were obtained using a microprobe system with lateral and depth resolution of ~ 2 μm. The specimen was scanned using a motorized stage, with

the intensities of the monoclinic and tetragonal peaks being measured as a function of distance from the crack, along lines normal to the crack, on the polished surface. The fraction of monoclinic phase was calculated from intensity ratios, using a calibration with x-ray measurements.[21] The calibration was done by comparing x-ray and Raman measurements from a series of specimens that were heat treated (1100°C) for several periods that caused systematic variations in the amounts of tetragonal-to-monoclinic transformation throughout the bulk.

3. RESULTS

3.1 Raman Calibration

The volume fractions of monoclinic phase in the series of heat treated specimens were evaluated from the integrated x-ray intensities from the monoclinic $(11\bar{1})$ and (111) and the tetragonal/cubic (111) peaks. The integrated intensities were derived from area measurements obtained by subtracting the background and fitting Pearson VII functions.[22] These results are compared with intensity ratios for the monoclinic (179 cm^{-1}) and tetragonal (145 cm^{-1}) Raman peaks in Fig. 1. Similar calibration curves were obtained from the area ratios using the combined peaks 179, 189 cm^{-1} for the monoclinic phase and 145, 265 cm^{-1} for the tetragonal phase. In all cases the calibration curves were nonlinear. In previous studies that used Raman measurements to evaluate the volume fraction of transformation in ZrO_2, a linear relation was assumed.

3.2 Crack Tip Zone Shape

Nomarski and conventional interference micrographs of the crack tip region in a high toughness (K_c = 16 MPa.$m^{1/2}$) material are compared in Fig. 2. The conventional

interference micrograph was obtained with the reference mirror set parallel to the undistorted surface, so that the fringes represent contours of constant normal surface displacement, separated by half of the wavelength of the monochromatic illumination ($\lambda/2$ = 2700Å). Surface uplift is detected to a distance of 1.5 mm from the crack plane. Moreover the shape of the zone ahead of the crack appears to be consistent with that expected for a zone defined by a contour of constant hydrostatic stress in the crack tip field. In the Nomarski interference micrograph (Fig. 2(b)) the same general surface uplift is evident adjacent to the crack, but the extent of uplift is not resolved as sensitively as in the conventional interference. In addition there is a general appearance in Nomarski interference of small transformation bands oriented at an angle of ~ 45° to the direction of crack growth, suggestive of a frontal zone defined by shear stress contours. The transformation bands are also visible in Fig. 2(a), as jagged outlines of the contours which would otherwise be smooth. It is clear from this micrograph that the bands are only a small perturbation on the overall displacements due to the transformation zone.

3.3 Initial Zone Development

The crack in Fig. 2 was grown initially from a saw notch at monotonically increasing stress intensity factor, following the resistance curve shown in Fig. 2(c): the critical applied stress intensity factor increased from an initial value of ~ 7 MPa.m$^{1/2}$ to a steady-state value of ~ 16 MPa.m$^{1/2}$ over a crack extension of ~ 2 mm. The corresponding increase in size of the transformation zone is clearly evident in the interference micrograph of Fig. 2(a): the outer limit of detectable surface displacement increased from an initial value of ~ 50 μm from the crack plane to 1.5 mm over the same region of crack growth.

3.4 Steady State Transformation Zone

Interference micrographs and measured surface displacements are shown in Fig. 3 for steady state cracks in two materials with steady state toughnesses of ~ 10 MPa $m^{1/2}$ and 16 MPa $m^{1/2}$. These micrographs were obtained with the reference mirror tilted so that the undistorted flat surface appears as parallel equally spaced fringes normal to the crack, and normal surface displacements appear as displacement of the fringes parallel to the crack. Large differences are evident in both the magnitude of the displacement at the crack plane and in the extent of the displacement field from the crack.

Corresponding Raman measurements of the fraction of transformed precipitates as a function of distance from the crack plane are shown in Fig. 4; intensity measurements (with background subtracted) from a single scan from the higher toughness material are shown in Figs. 4(a) and (b), whereas averaged data from several scans, converted to fraction transformed, are plotted as a function of $\sqrt{x}$ in Fig. 4(c). The shielding contributions to the fracture toughnesses (Eq. (2)) are proportional to the areas beneath the curves in Fig. 4(c). Several results from Fig. 4 are noteworthy:

(1) The minor peaks in the individual scans of Figs. 4(a) and (b) are genuine variations in the fraction of monoclinic and tetragonal phases, both within the transformation zone and remote from the crack. (Statistical fluctuations in the Raman intensities are smaller than these variations by a factor of approximately 5.) The spatial scale of the variations is approximately equal to the grain size.

(2) Complete transformation of all available tetragonal phase was never observed in regions adjacent to the crack; the intensity ratio $I_m/(I_m + I_t) \approx 0.8$ for the

high toughness material corresponds to a volume fraction of ~ 0.35, whereas the total fraction of tetragonal and monoclinic phases is ~ 0.45. Moreover, with the background monoclinic content subtracted, the largest volume fraction of transformation induced by the crack is only $f_o \simeq 0.25$.

(3) Both the fraction of transformation adjacent to the crack and the width of the transformation zone are larger in the higher toughness material than in the lower toughness material.

4. DISCUSSION

Previous calculations of crack tip shielding have assumed that the amount of transformation adjacent to the crack is equal to the fraction of tetragonal precipitates in the original material (~ 0.45).[7,8,18] This was based on transmission electron microscope observations which showed all precipitates transformed near the crack.[9,10] The results in Sect. 3.4 indicate that the fraction transformed is always less than this (maximum 0.35), thus suggesting that the reduced constraint of the thin TEM foil allows additional transformation.

The shape of the zone ahead of the crack has a large effect on the degree of shielding. For example, with a given zone width in the wake of the crack, a frontal zone defined by a contour of constant maximum crack tip shear stress results in a calculated toughness increase larger by approximately a factor of two than that due to a frontal zone defined by a contour of constant hydrostatic stress.[7] The results of Fig. 2 suggest that the latter shape is appropriate, i.e., the constant A in Eq. (1) is equal to 0.3. Local bands of transformation within the zone show strong contrast in Nomarski interference because of associated large local changes in slope of the surface. These have been taken

in the past to suggest a zone defined by a shear stress contour.[7] However, both the surface displacement and Raman measurements indicate that these bands are only a small fluctuation within the overall transformation zone (although it is noted that they may be critical as a mechanism for determining the total size of the zone).

The results in Fig. 4 can be used with Eq. (2) to evaluate the shielding stress intensity factor, ΔK_s, if we assume that the net transformation strain is purely dilational ($e^T = 0.04$) and that the frontal zone is in fact defined by a contour of constant dilational stress. The calculated values (using E = 200 GPa for Mg-PSZ) are shown on a plot of ΔK_s versus K_a in Fig. 5. Also shown is the relation

$$\Delta K_s = K_a - K_o \tag{3}$$

expected if the only toughening mechanism is shielding (K_o is the toughness of the overaged material). The calculated values of ΔK_s do not account for the measured toughness increases. Several potential causes of this discrepancy are: (1) partial reversibility in the transformation, (2) a shear component in the net transformation strain (i.e., transformation shear strain not fully relieved by twinning), and (3) contributions from other toughening mechanisms. Whether or not there is a shear component in the transformation strain can in principle be determined by comparison of measured surface displacement profiles such as Fig. 3 with displacements calculated using various trial combinations of dilation and shear in the strain e^T and the fraction of transformation, f(x), measured by Raman spectroscopy.[15] Preliminary calculations with e^T assumed to be purely dilational suggested that a component of shear may exist, especially in the region close to the crack; the calculated and measured displacements could be correlated well away from the crack, but the measured cusp-shaped profile near

the crack could not be reproduced by calculation, even when f(x) was taken to vary much more steeply than actually measured near the crack.[15] Further calculations with a shear component added to e^T are in progress to resolve this issue. Other in situ zone measurements during loading and unloading will also determine whether there are any changes in zone shape during unloading.

Finally, it is noteworthy that the interference measurements of surface uplift such as in Fig. 3 are a very sensitive indicator of changes in zone shape and toughness. The relative increases in the uplift, Δu, at the crack and in the width, w_o, of the zone are both larger than the relative toughness increase between the two materials; since Δu scales with fw and, from Eq. (1), $\Delta K_s \propto f \sqrt{w}$, both Δu and w should scale approximately with $(\Delta K_s)^2$ (since the variation in f is relatively small). This is consistent with the results in Fig. 3.

5. CONCLUSIONS

Characterization of transformation zones around cracks in several toughened Mg-PSZ ceramics by optical interference measurements of surface displacements and by Raman microprobe spectroscopy have provided the following results:

1. The shape of the frontal zone coincides approximately with contours of constant hydrostatic stress in the crack tip field.
2. The volume fraction of stress induced transformation from tetragonal to monoclinic phase is not uniform within the transformation zone.
3. Transformation of all of the tetragonal phase was never observed by Raman spectroscopy in regions adjacent to cracks, contrary to TEM

observations (the maximum transformation was approximately 80% of the original tetragonal phase).

4. The reductions in crack tip stress intensity factor (ΔK_S) due to shielding from the transformation zone were calculated from the Raman measurements of the zone profile, assuming that only the dilation component of the transformation remains (i.e., that the shear component is relieved by twinning). The values of ΔK_S were significantly smaller than the measured toughness increases. This result implies that either there are other toughening mechanisms operating, or there is a significant component of transformation shear strain that is not relieved by twinning.

ACKNOWLEDGMENTS

Funding for this work was supplied by the U.S. Air Force Office of Scientific Research under Contract No. F49620-85-C-0143.

Figure Captions

1. (a) and (b) Raman spectra from Mg-PSZ with mostly tetragonal (a) and monoclinic (b) precipitates.
(c) Comparison of Raman intensity ratios with the fraction of monoclinic phase evaluated from x-ray measurements.

2. (a) Optical interference micrographs (λ = 5400Å) of crack tip region and region of initial crack growth in high toughness Mg-PSZ (K_C = 18 MPa $m^{1/2}$). Reference mirror parallel to undistorted surface.
(b) Nomarski interference micrograph of crack tip in (a).
(c) Crack growth resistance curve for initial growth of crack in (a).

3. (a) Normal surface displacements, measured from optical interference micrographs, adjacent to steady-state cracks in Mg-PSZ with intermediate and high toughness (10 MPa $m^{1/2}$ and 16 MPa $m^{1/2}$).
(b) Optical interference micrographs from which measurements in (a) were obtained. Reference mirror tilted relative to undistorted surface.

4. (a) Intensities of monoclinic and tetragonal Raman peaks as a function of distance from the crack in the high toughness material of Fig. 3.
(b) Intensity ratios from (a).
(c) Fraction of material transformed from tetragonal to monoclinic phase by the cracks as a function of distance from the cracks in Fig. 3(b).

5. Shielding stress intensity factors calculated using the measurements of Fig. 4 for steady state cracks and plotted as a function of the steady state fracture toughness.

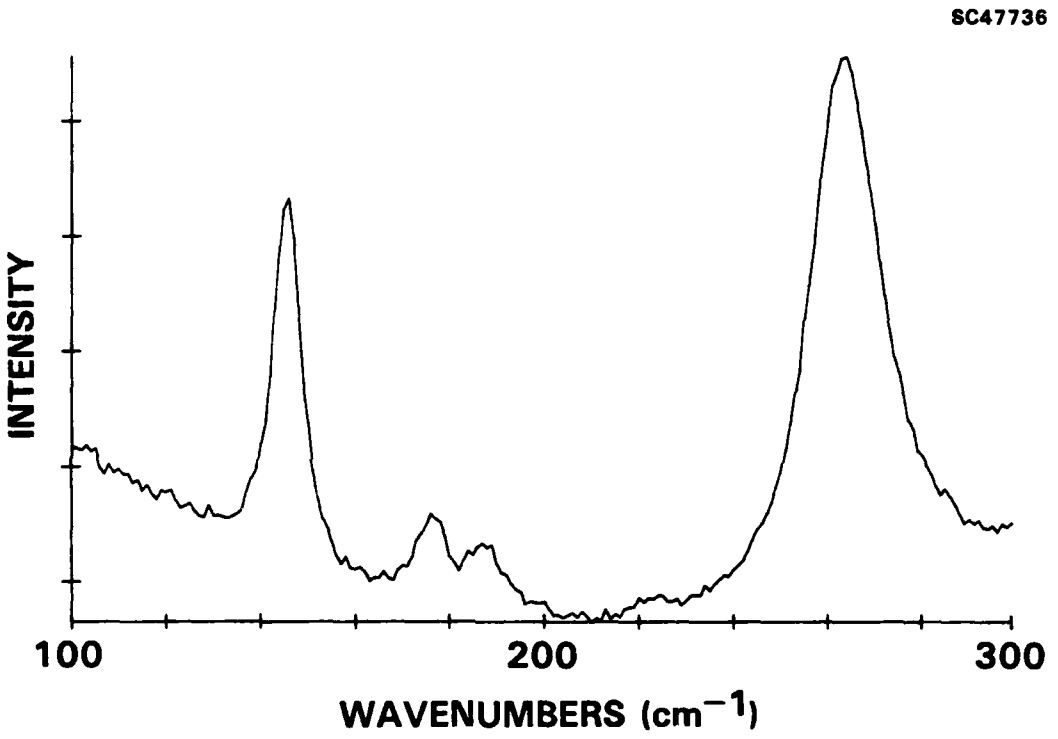

Fig. 1(a)

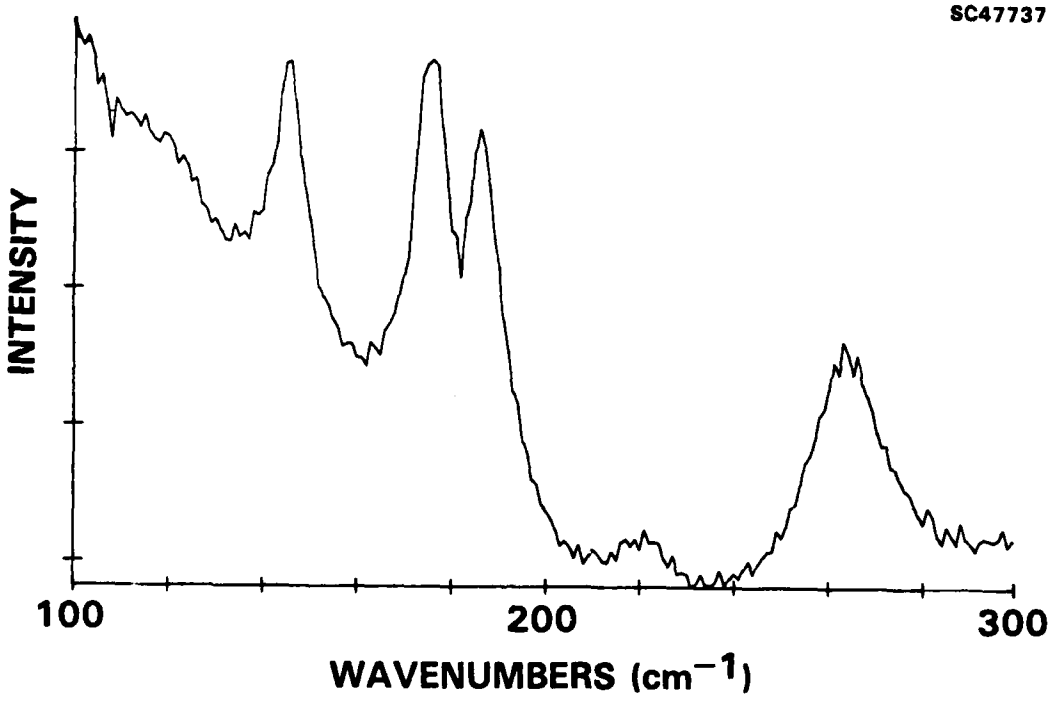

Fig. 1(b)

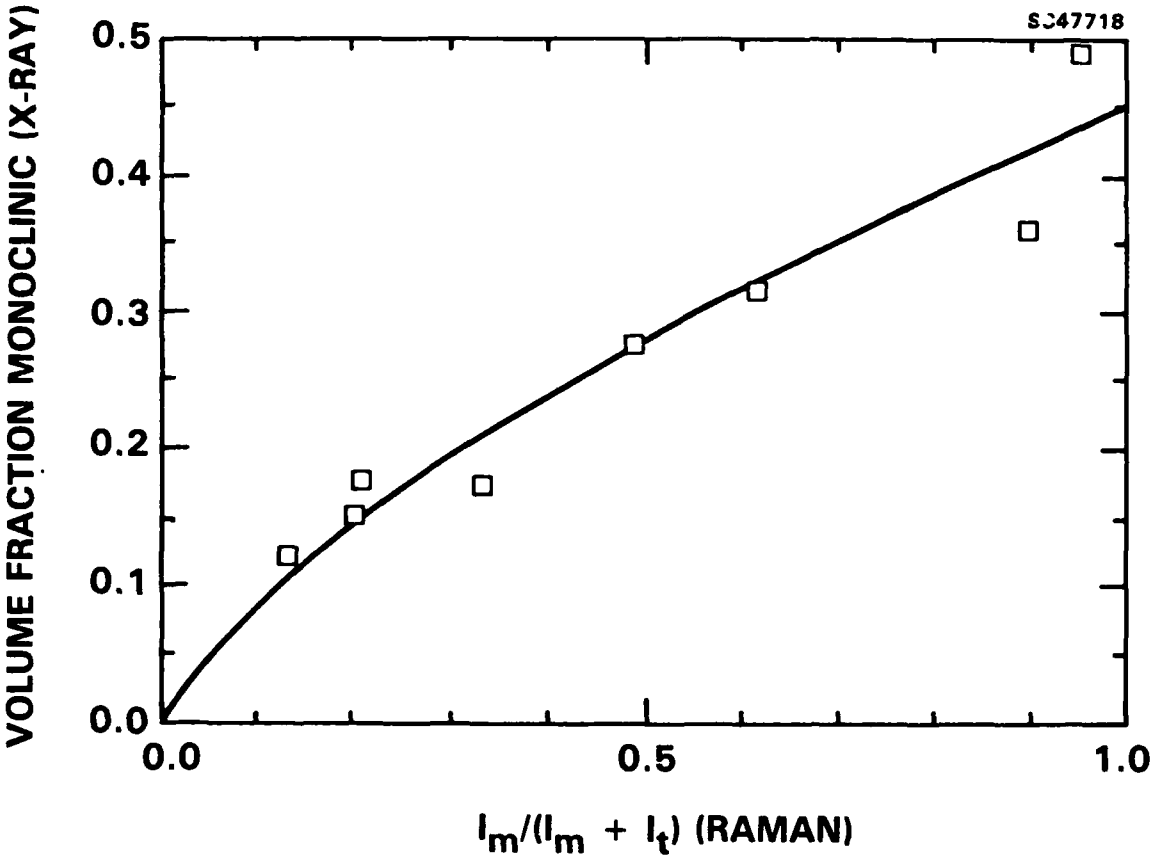
SC47718
VOLUME FRACTION MONOCLINIC (X-RAY)
0.5
0.4
0.3
0.2
0.1
0.0
0.0
0.5
1.0
$I_m/(I_m + I_t)$ (RAMAN)

Fig. 1(c)

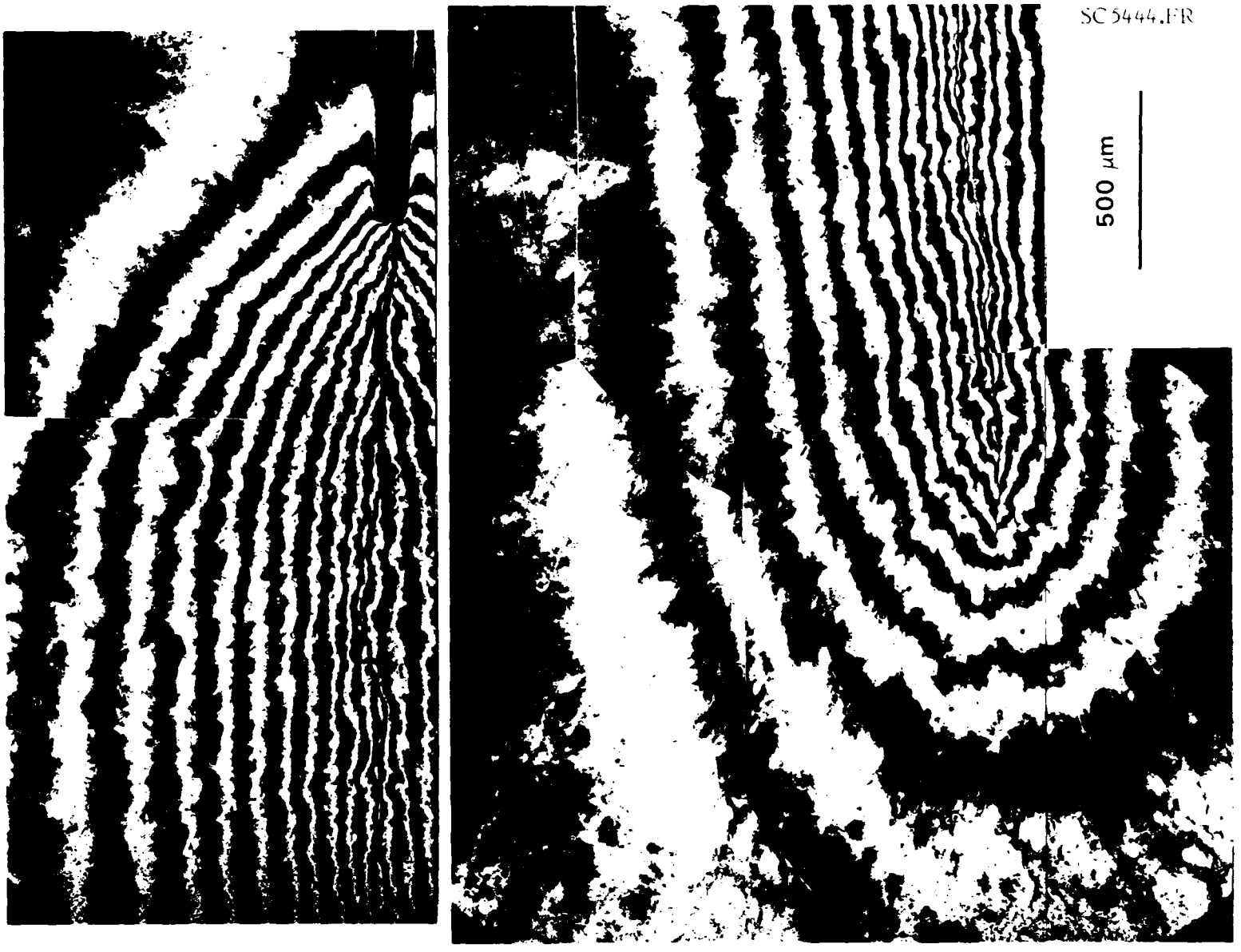

Fig. 2(a)

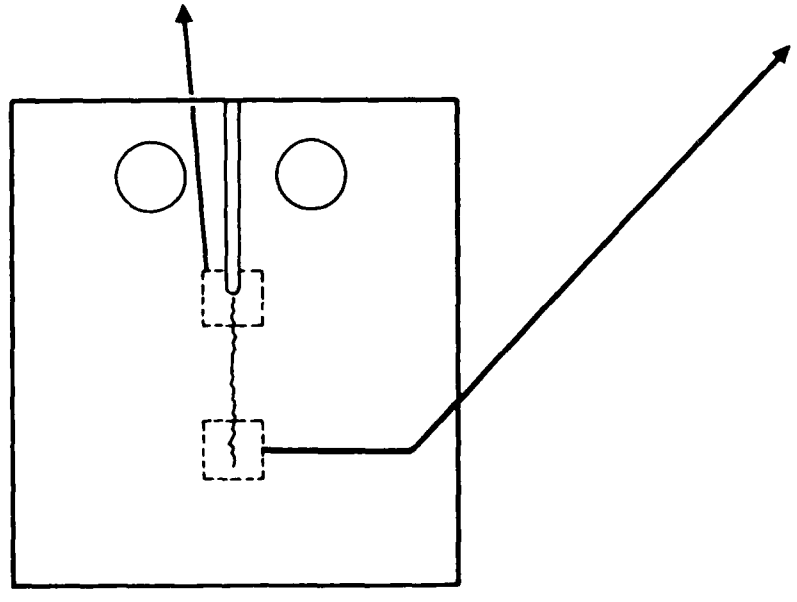

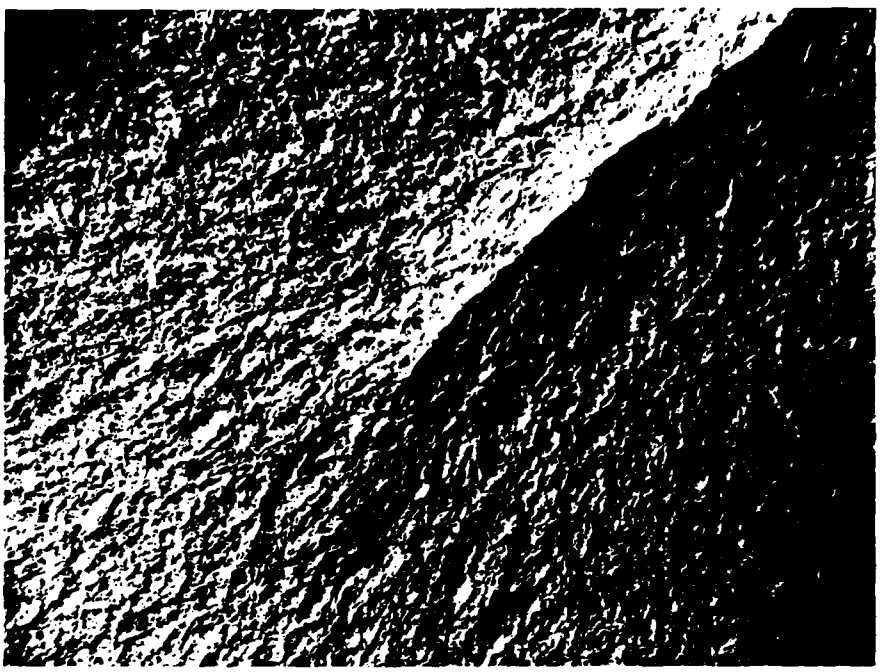

Fig. 2(b)

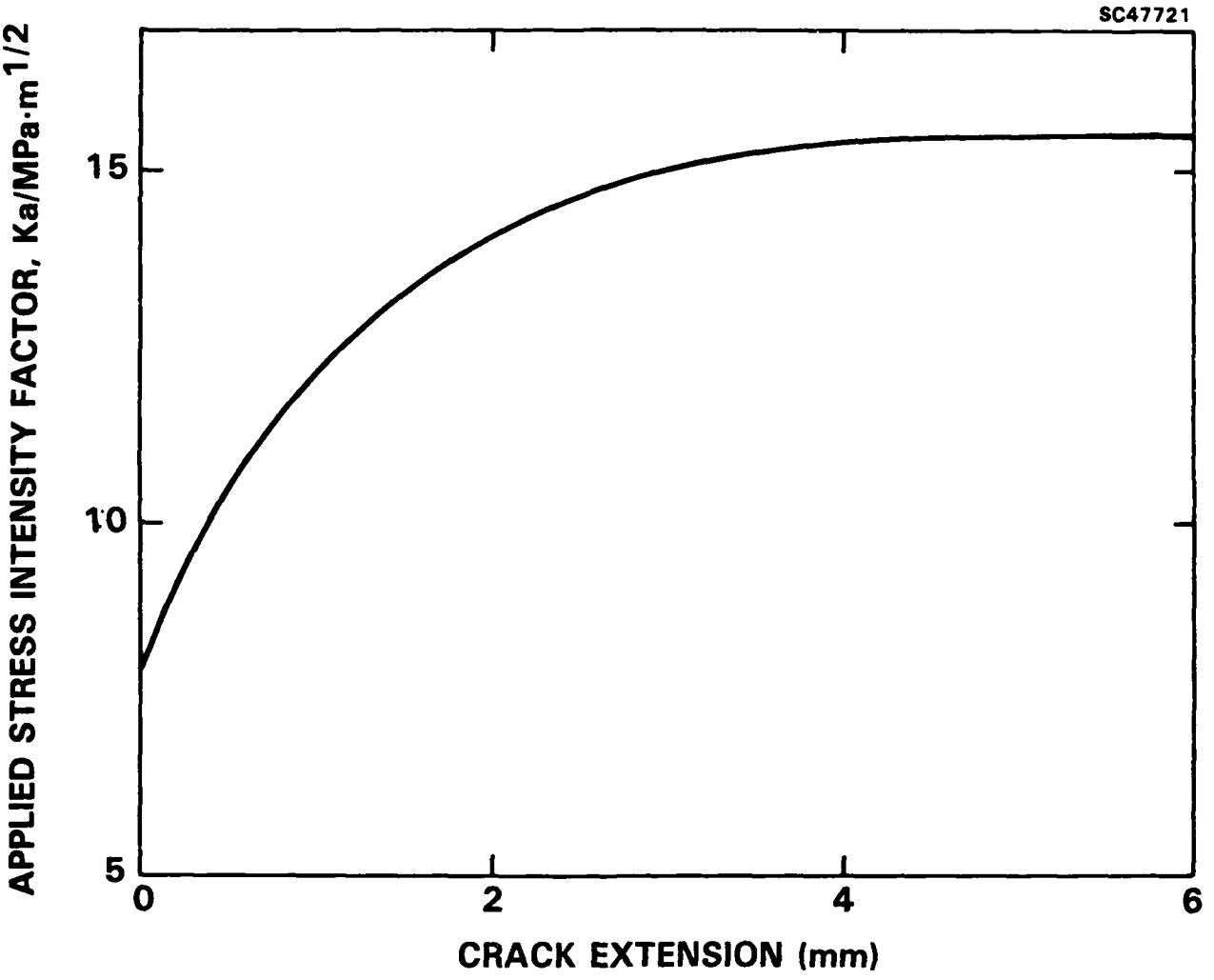
SC47721
APPLIED STRESS INTENSITY FACTOR, Ka/MPa·m^1/2
15
10
5
0
2
4
6
CRACK EXTENSION (mm)

Fig. 2(c)

SC5444.FR

SC47720

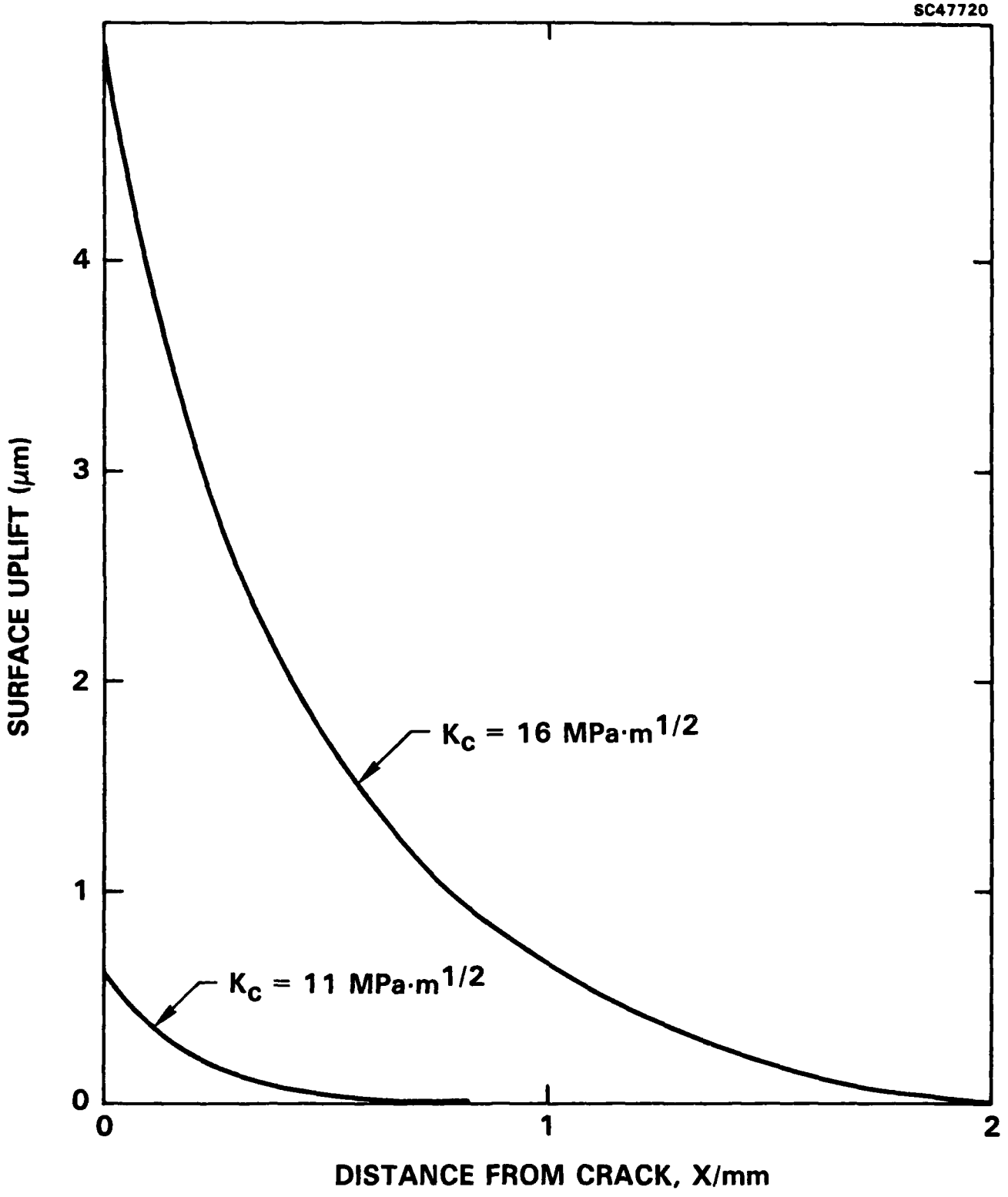

Fig. 3(a)

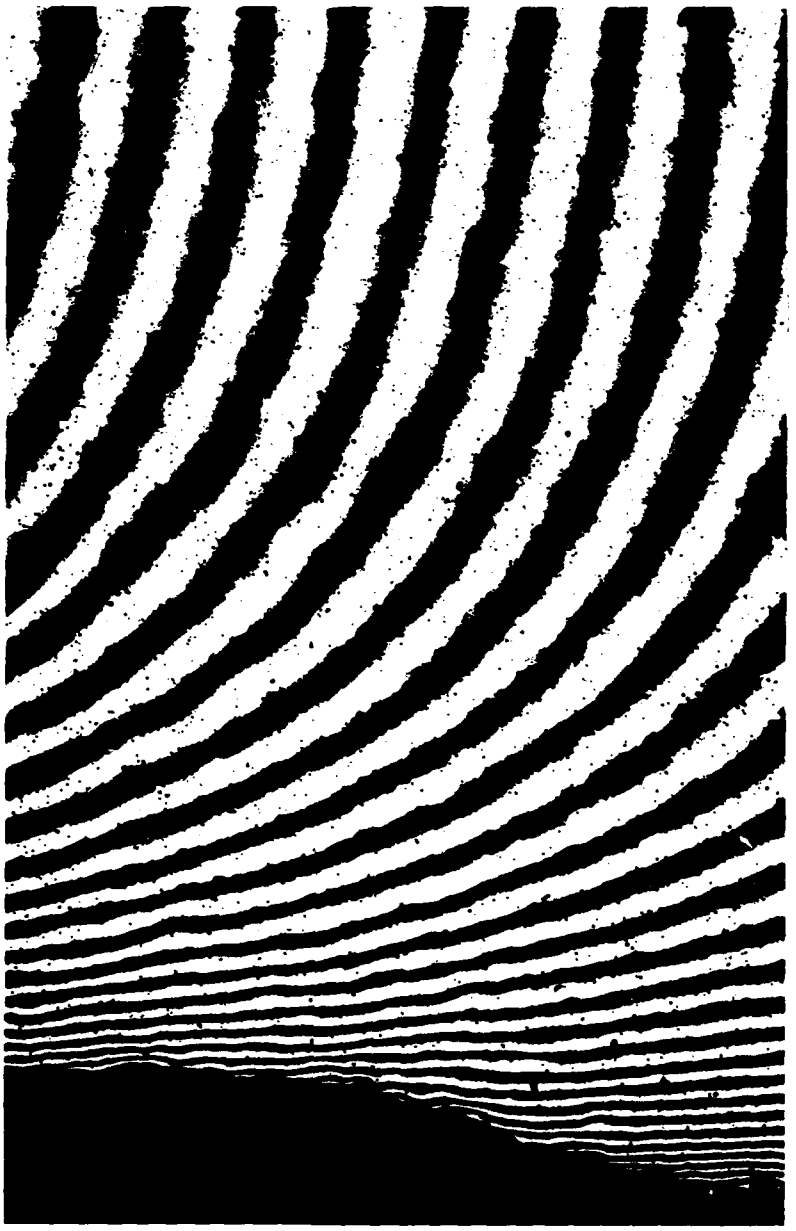

Fig. 3(b)

500 μm

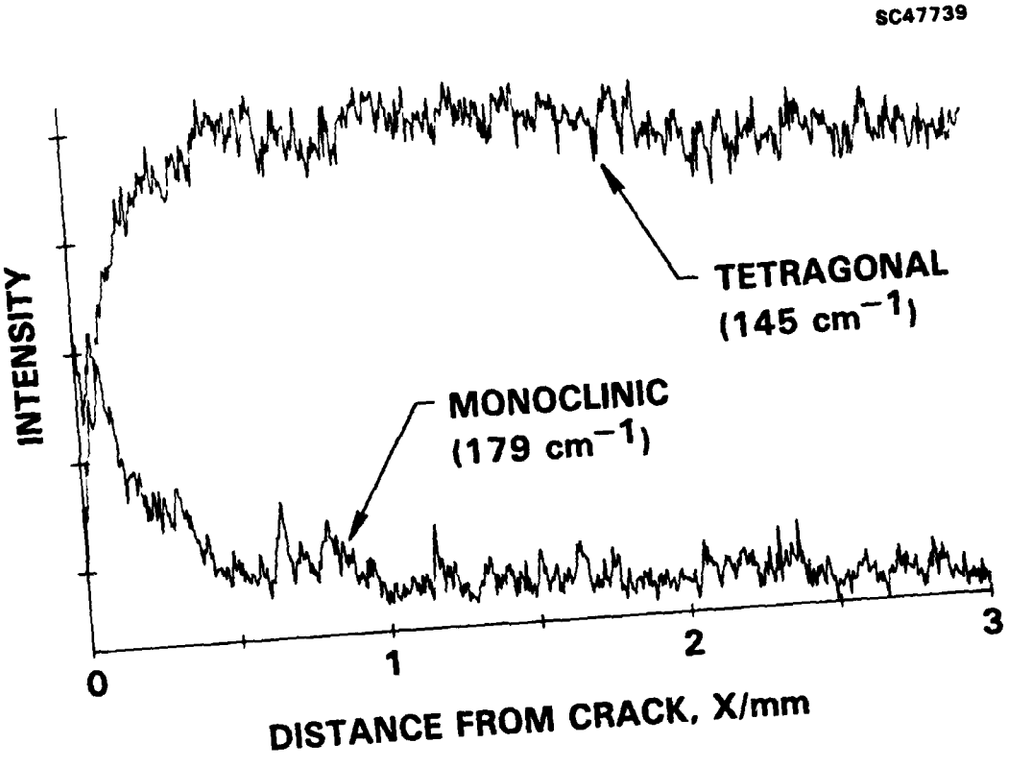
SC47739
INTENSITY
TETRAGONAL
(145 cm^{-1})
MONOCLINIC
(179 cm^{-1})
0
1
2
3
DISTANCE FROM CRACK, X/mm

Fig. 4(a)

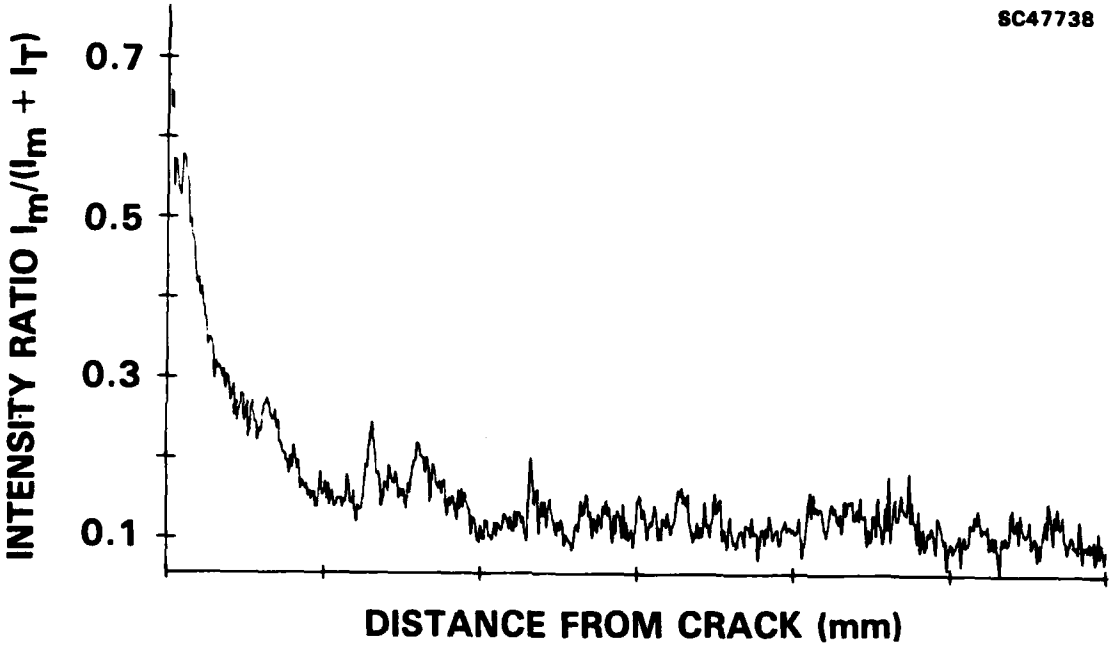
SC47738
INTENSITY RATIO $I_m/(I_m + I_T)$
0.7
0.5
0.3
0.1
DISTANCE FROM CRACK (mm)

Fig. 4(b)

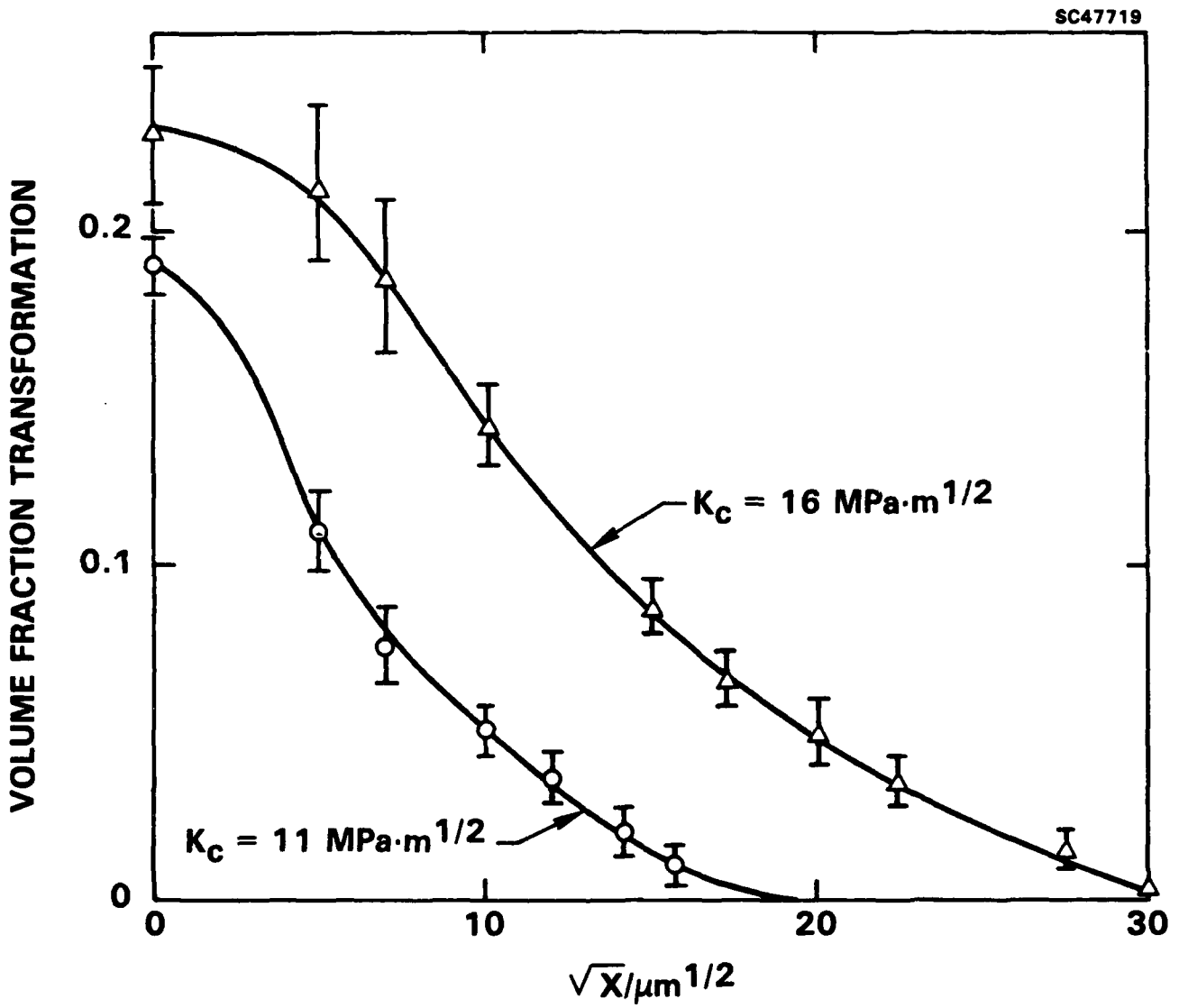
SC47719
VOLUME FRACTION TRANSFORMATION
0.2
0.1
0
0
10
20
30
K_c = 16 MPa·m$^{1/2}$
K_c = 11 MPa·m$^{1/2}$
$\sqrt{X}/\mu m^{1/2}$

Fig. 4(c)

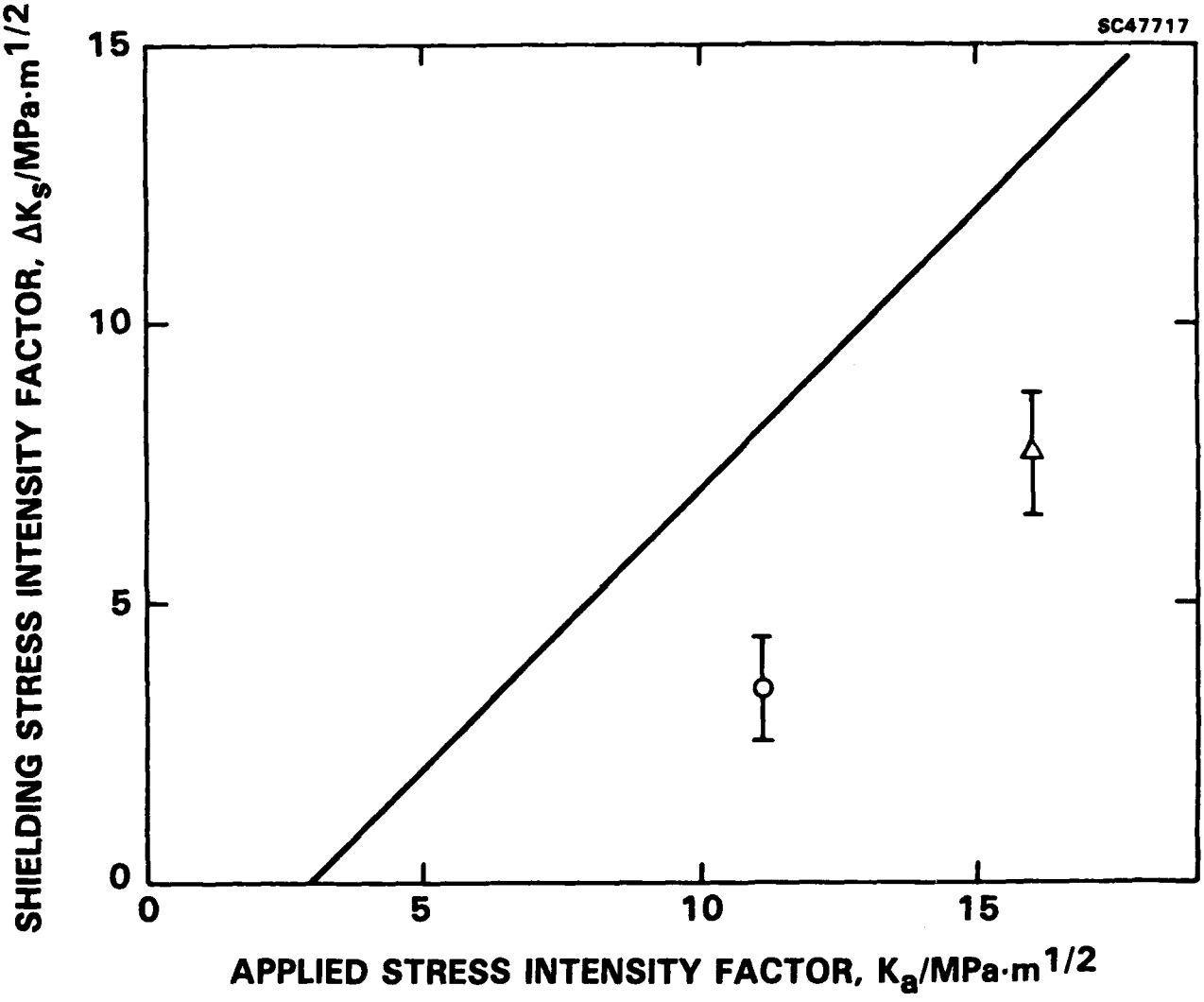
SC47717
SHIELDING STRESS INTENSITY FACTOR, ΔK_s/MPa·m$^{1/2}$
APPLIED STRESS INTENSITY FACTOR, K_a/MPa·m$^{1/2}$
0
5
10
15
0
5
10
15

Fig. 5